Article:
Zacharchenko, T, Kalverda, AP and Wright, SC orcid.org/0000-0002-3509-7506 (2021) Structural basis of Apt48 inhibition of the BCL6 BTB domain. Structure. ISSN 0969-2126

https://doi.org/10.1016/j.str.2021.10.010

Structural basis of Apt48 inhibition of the BCL6 BTB domain

Thomas Zacharchenko[1,3], Arnout P Kalverda[2] and Stephanie C Wright[1,4*]

[1] School of Biology and the Astbury Centre for Structural Molecular Biology, University of Leeds, Leeds LS2 9JT, UK

[2] School of Molecular and Cellular Biology and the Astbury Centre for Structural Molecular Biology, University of Leeds, Leeds LS2 9JT, UK

[3] Present address: Wellcome Trust Centre for Cell-Matrix Research, Faculty of Biology, Medicine and Health, University of Manchester, Manchester M13 9PT, UK

[4] Lead contact

* Correspondence: s.c.wright@leeds.ac.uk

SUMMARY

BCL6 is a transcriptional repressor that is deregulated in diffuse large B-cell lymphoma, and the peptide aptamer, Apt48, inhibits BCL6 by an unknown mechanism. We report the crystal structure of BCL6 in complex with an Apt48 peptide, and show that Apt48 binds to a therapeutically-uncharacterised region at the bottom of the BCL6 BTB domain. We show that the corepressor binding site of the BTB domain may conceptually be divided into two low-affinity peptide-binding regions. An upper region, the lateral groove, binds peptides in robust three-dimensional conformations, whereas a lower binding site is permissive to less-specific interactions. We show that, even with little sequence specificity, the interactions of the lower region are required for the high-affinity binding of the SMRT corepressor and other peptides to the BTB domain. This has relevance for the design of new BCL6 inhibitors and for understanding the evolution of corepressor interactions with the BTB domain.

INTRODUCTION

BCL6 (B cell lymphoma 6) encodes a transcriptional repressor that is a critical regulator of the adaptive immune response. It was originally identified as a locus that is translocated in diffuse large B-cell lymphoma (DLBCL) (Baron et al., 1993; Kerckaert et al., 1993; Ye et al., 1993), and is a promising therapeutic target for this disease (reviewed in (Cardenas et al., 2017; Ai et al., 2021)).

BCL6 is normally expressed at high levels in germinal centre (GC) B cells, which are the site of somatic hypermutation and class-switch recombination of the immunoglobulin genes (Kerfoot et al., 2011; Kitano et al., 2011). It enables rapid cell proliferation and prevents apoptosis in this setting of natural genomic instability. The down-regulation of BCL6 at the end of the GC reaction then allows terminal differentiation into memory B cells and long-lived antibody-secreting plasma cells. The overexpression of BCL6 in DLBCL thus contributes to malignancy by enhancing cell proliferation and DNA damage, and by preventing differentiation and apoptosis (reviewed in (Basso and Dalla-Favera, 2010, 2012; Hatzi and Melnick, 2014; Klein and Dalla-Favera, 2008)). BCL6 expression is also increased in the follicular helper T cells (Tfh) that provide help to B cells in the GC reaction (Nurieva et al., 2009), and it acts to suppress inflammatory cytokine expression in macrophages (Toney et al., 2000). Consistent with these roles, BCL6-deficient ($BCL6^{-/-}$) mice lack germinal centres, and die within a few weeks of birth from inflammatory disease that is driven by T cells and macrophages (Dent et al., 1997; Ye et al., 1997).

Many of the transcriptional properties of BCL6 are mediated by its N-terminal BTB (bric-à-brac, tramtrack and broad complex; also known as POZ, poxvirus and zinc finger) domain (Seyfert et al., 1996), that interacts with the transcriptional corepressors NCoR, SMRT and BCOR (Dhordain et al., 1997; Huynh and Bardwell, 1998; Huynh et al., 2000; Wong and Privalsky, 1998). Different corepressors are associated with BCL6-transcription complexes at individual gene promoters and enhancers (Hatzi et al., 2013), and the various domains of BCL6 are associated with discrete physiological functions (Huang et al., 2014; Huang et al., 2013). The BTB domain is specifically required for cell proliferation and tolerance to DNA damage in the GC reaction, and strategies to target BCL6 have therefore focussed on inhibiting corepressor interactions with this region (reviewed in (Cardenas et al., 2017)); the phenotypes of mouse models predict that this approach should interfere with germinal centre function in DLBCL cells, without affecting BCL6 activities in T cells and macrophages (Huang et al., 2013). The BTB domain also mediates interaction with the BTB-domain transcription factor MIZ1, leading to the repression of MIZ1 target genes, such as *BCL2* (Saito et al., 2009) and *CDKN1A* (Phan et al., 2005), that are relevant in DLBCL.

Corepressors interact with the BTB domain via their intrinsically-disordered 17-residue BCL6-binding domain (BBD), and whereas the BBD sequences of NCoR and SMRT are virtually identical, that of BCOR shares no similarity (Ahmad et al., 2003; Ghetu et al., 2008). Crystallographic studies have shown that BBD sequences interact with an extended, largely hydrophobic lateral groove that is formed at the interface of the domain-swapped BTB dimer, and also with the β1-strand at the "bottom" (depicted in **Figure S1A**). A

corepressor molecule binds to the each of the two equivalent lateral grooves of the symmetrical dimer, with each corepressor interacting with residues from both BTB chains. The BBD sequences of SMRT and BCOR bind to the lateral groove with different backbone conformations, and make different main-chain and side-chain contacts with BTB residues (Ahmad et al., 2003; Ghetu et al., 2008). The lateral groove is thus a region of tremendous plasticity that can accommodate diverse corepressor sequences and also non-physiological peptide sequences identified in screening approaches.

Initial approaches to target the BTB domain used peptide inhibitors based on natural corepressor sequences, and these agents antagonised BCL6 function in cell-based assays and animal models (Cerchietti et al., 2009; Ghetu et al., 2008; Polo et al., 2004). More recently, an unbiased phage-display search for BTB-interacting peptides led to the identification of F1324, which binds the lateral groove with a higher affinity than the natural corepressors (Sakamoto et al., 2017). The lateral groove has also been targeted by small molecule inhibitors identified by computational selection or NMR screening (for example (Cardenas et al., 2016; Cerchietti et al., 2010; Kamada et al., 2017; Yasui et al., 2017)), and by a natural compound identified in an unbiased screen for inhibitors of corepressor-dependent activities (Evans et al., 2014). Most of these molecules target an aromatic pocket at the "top" of the lateral groove, although recently-developed high-affinity compounds also interact with the HDCH site (BCL6 residues H14, D17, C53, H116) located further down this region (Cheng et al., 2018; depicted in **Figure S1B**). A different approach for identifying BTB-domain inhibitors used yeast two-hybrid assays to search for aptamers that probe the surface of the protein for functionally important regions. This led to the identification of Apt48, which specifically antagonised BCL6 function both *in vitro* and in cultured cells (Chattopadhyay et al., 2006). The region of the BTB domain that binds Apt48 was not structurally characterised, although the interaction was notably unaffected by the lateral groove mutation, N21K (depicted in **Figure S1B**), that abolishes the interaction of BCL6 with corepressors. This suggested that Apt48 might be targeting BCL6 in a manner distinct from other inhibitors, thereby identifying an unexplored region of the BTB domain that has therapeutic relevance.

In order to resolve this, we solved the crystal structure of the BCL6 BTB domain in complex with an Apt48 peptide, and characterised this interaction biophysically. Apt48 interacts with low affinity at a hydrophobic face at the bottom of the BTB domain, in a region distinct from the upper lateral groove that is targeted by other inhibitors. This led us to examine the role of the lower hydrophobic face in the interaction of BCL6 with the SMRT corepressor, and we showed by mutagenesis that this region is required for high-affinity binding. We also found that a known "truncated" SMRT-based peptide inhibitor interacts with low affinity at the upper portion of the lateral groove. A variety of short sequences interact with the lower hydrophobic face, and this suggested that the high-affinity interaction of longer peptides with the BTB domain involves the synergistic action of the two weak binding sites. To test this hypothesis, we made a hybrid BTB-binding peptide (HBP) that comprised a "truncated" SMRT-based warhead peptide (Cerchietti et al., 2009) fused to a sequence that binds the lower hydrophobic face. The HBP peptide bound to the BTB

domain with a similar affinity to the natural SMRT corepressor peptide, and in a similar conformation. This led us to demonstrate by ITC that a variety of potential sequences, including the frequently used TAT nuclear localisation sequence, can synergistically bind BCL6 in concert with the warhead peptide. Our data emphasise the importance of the lower region of the BTB domain-binding site, and have relevance for the design of therapeutic inhibitors that interact with this region.

RESULTS

Structure of the BCL6^{BTB-TM}/Apt48 complex

The peptide aptamer, Apt48, was originally identified in a yeast two-hybrid screen for random sequences that interact with the BCL6 BTB domain (Chattopadhyay et al., 2006). Apt48 comprised a 10-amino acid sequence inserted into an exposed loop of an *E.coli* thioredoxin scaffold; the scaffold alone did not interact with BCL6, and Apt48 did not interact with other BTB domains tested. In yeast two-hybrid assays, Apt48 interactions were not affected by the BTB domain mutation, N21K (depicted in **Figure S1B**), which abolishes the interaction of corepressors with the lateral groove, suggesting that it binds in a distinct manner. The interaction of Apt48 with short fragments of BCL6 was also tested in yeast two hybrid assays, suggesting the involvement of a beta-sheet region at the top of the BTB domain (Chattopadhyay et al., 2006); however, these BCL6 fragments would not have reflected the true molecular context of an intact BTB domain. It has also been speculated that Apt48 might interact with a charged pocket of unknown function located at the top of the BTB domain (Cardenas et al., 2017). Since the interaction between the BCL6 BTB domain and Apt48 had not been studied by biophysical approaches, we sought to characterise this. Secondary structure predictions using the PSIPRED server indicated that the Apt48 peptide is unstructured in the context of the thioredoxin fold **(Figure S2A)**. For our studies, we therefore used the synthetic peptide, ^{1}GPHGPRDWCLFGGP^{14}, which corresponds to the Apt48 sequence together with the flanking scaffold residues, GP. For initial experiments, we used the BCL6 BTB domain triple mutant (BCL6^{BTB-TM}) that contains the solubility-enhancing mutations (C8Q, C67R and C84N) previously used for crystallographic studies (Ahmad et al., 2003; depicted in **Figure S1B**).

Using the previously published backbone resonance assignment of BCL6^{BTB-TM} (Lin et al., 2018), we mapped the chemical shift perturbations (CSPs) of the Apt48 interactions with ^{15}N-labelled BCL6^{BTB-TM} using ^{1}H-^{15}N TROSY HSQC. Spectra were collected under identical conditions to the published assignment, allowing unambiguous transfer of 95.4% of the assignments to our spectra; unassigned residues are listed in **Figure S2C.** Overall, the induced spectral changes were small and indicative of a direct low-affinity protein-protein interaction **(Figures 1A, S2B and S2C)**; this contrasts the interaction between ^{15}N-labelled BCL6^{BTB-TM} and a previously described SMRT BBD peptide **(Figure S2D)** that is known to interact with micromolar affinity (Ahmad et al., 2003). The largest CSPs observed upon Apt48 binding, as determined by being greater than

2σ of the mean chemical shift change, were localised to I9, Q10, L25, G55, L56, E115, V117, T120 and F124 **(Figure S2C)**. Many of these spectral changes were localised to a hydrophobic face that encompasses residues of the β1-strand and the C-terminal α6 helix; others are in the adjacent exposed hinge region between the α2 and α3 helices (**Figure 1B**). This result was unexpected, as previous reports of Apt48 function had suggested a binding site that is independent of the lateral groove (Chattopadhyay et al., 2006).

To reveal the structural basis for this interaction, we solved the 1.63Å crystal structure of $BCL6^{BTB\text{-}TM}$ in complex with the Apt48 peptide. The structure contained one BCL6 BTB domain homodimer bound to two Apt48 molecules in the asymmetric unit **(Figure 2A and Table 1)**. Only six residues of the Apt48 peptide, ^{7}DWCLFG^{12}, were resolved in the structure, with the electron density of side chains being clearly visible in the F_o-F_c difference map and simulated annealing (SA) omit map **(Figure S3A)**. Residues W8, C9 and L10 of the Apt48 peptide form a short twisted antiparallel β-sheet with the β1-strand of the BTB domain **(Figures 3B, S3C and S3D)**, burying W8 of the Apt48 hexapeptide in the core of a lower hydrophobic face that comprises residues I9 and F11 from the β1-strand and T120 and F124 of α6 **(Figures S3B and S3D)**; this is therefore consistent with our chemical shift mapping. The side chains of the BTB domain residues R13 and H116' are oriented such that they partially block the upper portion of the lateral groove **(Figure S3B);** this orientation has also been observed in BTB domain structures obtained in the absence of lateral groove-binding corepressor peptides (Ahmad et al., 2003). Within the crystal, the Apt48 peptide is also involved in a crystallographic contact with Y111 of a symmetry-related BTB homodimer. However, the chemical shift data does not support the existence of multiple APT48 binding sites, with Y111 remaining relatively unchanged at high peptide excess **(Figures S2B and S2C).**

Given the low affinity of the interaction between Apt48 and BCL6, we reasoned that, in solution, the interface might be extended beyond the region of the peptide captured in our crystal structure. To establish the relative contribution of Apt48 residues involved in its interaction with BCL6, we tested several Apt48 mutants; this would also further verify the hydrophobic face as the main binding site of Apt48 in solution. We tested the interaction of ^{15}N-labelled $BCL6^{BTB\text{-}TM}$ with three variants of the Apt48 sequence that were designed based on the crystal structure: Apt48P2R, that has a mutation located N-terminal to the residues resolved in the crystal structure, Apt48W8R, that contains a mutation in a BCL6-interacting residue, and Apt48ΔN that contains only those residues that were resolved in the crystal structure. Although the Apt48ΔN peptide had limited solubility, only allowing a comparison of HSQC data up to a 3-fold molar excess of peptide, we showed that Apt48P2R and Apt48ΔN both bound to $BCL6^{BTB\text{-}TM}$ with a similar affinity to the original Apt48 sequence, with the same subset of peaks affected to a similar magnitude **(Figure 2C)**. The Apt48W8R mutant did not bind to $BCL6^{BTB\text{-}TM}$, indicating a critical role of the hydrophobic side chain of W8 **(Figure 2C)**. These data are consistent with our crystal structure and initial NMR mapping, and we consider it likely that some of our observed resonance shift changes (BCL6 residues

G55, L56, E115, V117) are indirect. We conclude that Apt48 interacts with a lower hydrophobic face at the bottom of the BTB domain, explaining why this interaction was unaffected by the BCL6 N21K mutation in the original yeast two-hybrid experiments of Chattopadhyay et al. (Chattopadhyay et al., 2006).

The hydrophobic face of the BCL6 BTB domain is required for interaction with the SMRT corepressor

The interaction of the Apt48 peptide with BCL6 was abolished by the mutation of Apt48 W8. Structural superposition of the $BCL6^{BTB\text{-}TM}$/Apt48 complex with the BCL6-corepressor peptide complex, $BCL6^{BTB\text{-}TM}$/$SMRT^{BBD}$ (Ahmad et al., 2003), revealed that the region of BCL6 that interacts with Apt48 W8 is occupied by the buried corepressor residue, SMRT E1420, in $BCL6^{BTB\text{-}TM}$/$SMRT^{BBD}$; engagement of SMRT is facilitated by the SMRT E1420 side chain pointing away from the BTB β1-strand, with the γC being located at the hydrophobic interface. Early pull-down studies with bacterial-expressed proteins showed that SMRT residues 1417–1421 were required for interaction with the BCL6 BTB domain (Ahmad et al., 2003), and fluorescence polarisation competition assays showed that the interaction of the $SMRT^{BBD}$ peptide with BCL6 is abolished by the mutation of SMRT E1420 (Ghetu et al., 2008). The hydrophobic face at the bottom of the lateral groove may therefore be an important determinant of BTB domain interactions both with Apt48 and with the natural corepressor, SMRT.

To analyse the role of this region in mediating SMRT interactions, we used ITC to measure the binding of the $SMRT^{BBD}$ peptide to BCL6 BTB domain mutants. The BTB domain triple mutant, $BCL6^{BTB\text{-}TM}$ (C8Q C67R C84N), used in previous studies contains the C8Q mutation in the β1-strand that interacts with Apt48 and corepressors. We therefore made a BTB domain double mutant ($BCL6^{BTB\text{-}DM}$), which has a wild-type β1-strand whilst retaining the solubility-enhancing mutations C67R and C84N. The $SMRT^{BBD}$ peptide bound to $BCL6^{BTB\text{-}TM}$ and $BCL6^{BTB\text{-}DM}$ with similar affinity, with K_ds for the interactions being 5.83 µM ± 0.17 (N = 0.98 ± 0.14, ΔH = -9.96 kcal/mol ± 1.53, TΔS = -2.81 kcal/mol ± 1.55 and ΔG= -7.15 kcal/mol ± 0.01) and 7.71 µM ± 1.08 (N = 1.00 ± 0.05, ΔH = -10.68 kcal/mol ± 0.39, TΔS = -3.69 kcal/mol ± 0.29 and ΔG = -6.99 kcal/mol ± 0.09) respectively **(Figure 3)**. This is in agreement with other studies that suggested that the C8Q mutation does not affect corepressor binding to the BTB domain (Ahmad et al., 2003; Kamada et al., 2017). We also showed that Apt48 interacts with ^{15}N-labelled $BCL6^{BTB\text{-}DM}$ using ^{1}H-^{15}N TROSY HSQC **(Figure S4A),** with larger changes than observed for the interaction with ^{15}N-labelled $BCL6^{BTB\text{-}TM}$. Although this might suggest that the binding of Apt48 was compromised by the C8Q mutation, we were unable to detect heat release during ITC titration of the Apt48 peptide with $BCL6^{BTB\text{-}DM}$ **(Figure S4B**). This confirmed that the interaction of Apt48 with the BTB domain is weak, and could not therefore be measured under the experimental conditions of the ITC.

To disrupt the lower hydrophobic face of the BTB domain, we introduced the I9E and F11E mutations into $BCL6^{BTB\text{-}DM}$ to create $BCL6^{BTB\text{-}DM\text{-}I9E}$ and $BCL6^{BTB\text{-}DM\text{-}F11E}$. $BCL6^{BTB\text{-}DM\text{-}I9E}$ and $BCL6^{BTB\text{-}DM\text{-}F11E}$ had identical elution

volumes to $BCL6^{BTB\text{-}DM}$ on size-exclusion chromatography, indicating that the I9E and F11E mutations did not disrupt the BTB dimer interface **(Figure S4C)**, and ^{1}H-NMR spectra showed that these proteins were folded, having proton chemical shift dispersions similar to that of the $BCL6^{BTB\text{-}TM}$ protein (data not shown). We found that the $SMRT^{BBD}$ peptide did not interact with either $BCL6^{BTB\text{-}DM\text{-}I9E}$ or $BCL6^{BTB\text{-}DM\text{-}F11E}$ as assessed by ITC **(Figure 3)**, indicating that the lower hydrophobic face of the BTB domain is important for SMRT binding.

The ^{1}GRSIHEIPR^{9} sequence directs peptide recruitment to the lateral groove

Early peptide inhibitors of BCL6 were based on the 17-residue BBD sequences of SMRT and BCOR that interact both with the lateral groove and with the β1-strand at the bottom of the BTB domain. More recent inhibitors based on the $SMRT^{BBD}$ have included just the 9-amino acid warhead region, ^{1}GRSIHEIPR^{9}, which would be predicted to interact with the aromatic pocket region in the upper part of the lateral groove (Cerchietti et al., 2009), but not with the lower hydrophobic face that is involved in the interaction with Apt48. The affinity of the ^{1}GRSIHEIPR^{9} peptide for BCL6 has not been reported, and, as with the Apt48 peptide, we were unable to detect any heat release during ITC titrations of a ^{1}GRSIHEIPR^{9} peptide into $BCL6^{BTB\text{-}DM}$ **(Figure 4A).**

We also examined the interaction of ^{1}GRSIHEIPR^{9} with $BCL6^{BTB\text{-}TM}$ and $BCL6^{BTB\text{-}DM}$ using ^{1}H-^{15}N TROSY HSQC **(Figures S5A, S5B and S5C).** Examination of the CSPs of the interactions between $BCL6^{BTB\text{-}TM}$ and the ^{1}GRSIHEIPR^{9} peptide provided a revealing insight into ^{1}GRSIHEIPR^{9} function **(Figures 4B, S5A and S5B)**. The ^{1}GRSIHEIPR^{9} peptide induced a larger range of chemical shift changes than the Apt48 peptide, with more peaks perturbed in α1 (for example, H14, A15, N23, R26, R28) and α2-α3 residues (for example, V49, M51, F57, I60, T62) and significant exchange broadening in residues localised to the upper region of the lateral groove (for example V18 and C53). Interestingly, there was also exchange broadening of Q10 and F11 (but not I9); this is consistent with the interaction of SMRT G1422 with BCL6 residues Q10 and F11 when in the context of the full SMRT co-repressor BBD (Ahmad et al., 2003). In contrast, the residues that were most affected by Apt48 binding were localised to the lower hydrophobic face and α6-helix. Notably, Apt48 induced no chemical shift changes on the V49 and T62 residues that are located in upper portion of the lateral groove **(Figure S2B)** and that are changed upon the binding of SMRT, ^{1}GRSIHEIPR^{9}, or the small-molecule inhibitor FX1 (Cardenas et al., 2016). The ^{1}GRSIHEIPR^{9} and Apt48 sequences therefore interact with low affinity at the upper and lower portions of the BTB domain binding site respectively.

Our NMR analysis showed that the ^{1}GRSIHEIPR^{9} peptide binds the BCL6 BTB domain with low affinity. However, multiple *in vivo* studies have shown that this truncated SMRT BBD sequence is a potent inhibitor of BCL6 function in biological assays (Cerchietti et al., 2009), highlighting a potential discrepancy between the *in vivo* effect and the *in vitro* binding affinity. In work describing the specific inhibitory function of

^{1}GRSIHEIPR^{9} *in vivo,* this sequence was used in the context of a fusion to the nuclear localization signal of the HIV TAT protein, thereby creating the peptide YGRKKRRQRRRGGRSIHEIPR (TAT-GRSIHEIPR). The TAT sequence shares no similarity with the N-terminal portions of the corepressor BBD sequences that interact with the BTB domain β1-strand (Ahmad et al., 2003; Ghetu et al., 2008; Zacharchenko & Wright 2021), and we initially considered the TAT sequences unlikely to contribute to the overall binding affinity of TAT-GRSIHEIPR. In addition, fluorescence polarization competition assays had indicated that residues in the N-terminal portion of the SMRT and BCOR BBDs were important for BCL6 binding (Ghetu et al., 2008), which might be consistent with our observed low affinity binding of ^{1}GRSIHEIPR^{9}. It was, however, relevant to determine whether ^{1}GRSIHEIPR^{9} is a low-affinity, yet effective, peptide inhibitor, or whether this sequence forms part of a longer, composite binding site when in the context of the TAT-GRSIHEIPR fusion.

We used ITC to examine the contribution of the TAT sequences to the affinity of the TAT-GRSIHEIPR peptide for BCL6$^{BTB\text{-}DM}$. Comparison of ITC isotherms revealed that whereas ^{1}GRSIHEIPR^{9} produced little or no heat release in solution **(Figure 4A),** the extended TAT-GRSIHEIPR peptide bound with a K_d of 13.54 μM ± 1.34 (N = 1.22 ± 0.16, ΔH = -3.42 kcal/mol ± 1.96 , TΔS = 3.22 kcal/mol ± 2.02 and ΔG = -6.64 kcal/mol ± 0.06) **(Figure 4C)**, which is a similar order of magnitude to the K_d of the SMRT corepressor peptide **(Figure 3)**. This unexpected result led us to postulate that the GRSIHEIPR sequence can direct the recruitment of a variety of fused peptide sequences to the lower portion of the BTB domain. The ability of this latter BTB region to interact with different sequences is supported by the recent observation of a low-affinity interaction of the BCL6 hydrophobic face with a previously uncharacterized co-repressor sequence *in vitro* (Zacharchenko and Wright, 2021). Our data therefore demonstrate that the lower hydrophobic face of the BCL6 BTB domain is a promiscuous binding site capable of a variety of protein-protein interactions.

A hybrid BTB-binding peptide (HBP) interacts with the lateral groove

Synergistic protein-protein interactions can occur when two low-affinity binding sequences are covalently joined to form a high affinity peptide (for example, Sakamoto et al., 2017). We hypothesised that, in principle, a variety of sequences can be recruited to the BTB domain when part of a composite peptide that contains ^{1}GRSIHEIPR^{9}. The BTB domain β1-strand can interact with peptide sequences in either a parallel or anti-parallel orientation, and we also considered that peptide side-chains might be relevant in determining interactions with this region (Merkel et al., 1999). The natural corepressors interact with the BTB domain β1-strand in a parallel orientation, whereas the interaction with Apt48 residues (DWCLFGGP) is anti-parallel. We therefore reasoned that the β1-strand might interact with an inverted Apt48 sequence, PGGFLCWD, in a parallel orientation when these residues are fused to the N-terminus of the ^{1}GRSIHEIPR^{9} peptide. We therefore made a hybrid peptide (HBP), PGGFLCWDGRSIHEIPR **(Figure 5A)**, and reasoned that residue W7 of HBP would interact with the same BTB residues as SMRT^{BBD} residue E1420 and Apt48 residue

W8. The interaction of the HBP peptide with BCL6^{BTB-DM} was measured by ITC, and showed a K_d of 6.51 µM ± 2.10 (N = 0.92 ± 0.13, ΔH = -4.88 kcal/mol ± 0.84 , TΔS = 2.20 kcal/mol ± 0.63 and ΔG= -7.08 kcal/mol ± 0.21) **(Figure 5B)**, which is similar to the interaction of BCL6^{BTB-DM} with SMRT^{BBD}**;** ^{1}H-^{15}N TROSY HSQC of BCL6^{BTB-TM} showed that addition of the HBP peptide led to resonance shift changes comparable to those observed using SMRT^{BBD} **(Figure S6A).**

To establish the molecular basis of the interaction between the HBP peptide and BCL6^{BTB-TM}, we solved the structure of the BCL6^{BTB-TM}/HBP complex to 2.13Å resolution **(Figures 5C, 5D and Table 1)**. The HBP peptide is well-resolved in the structure, with all side chains clearly visible in the F_0-F_C difference map and SA omit map **(Figure S6B)**. The HBP peptide interacts with BCL6^{BTB-TM} in the same manner as SMRT^{BBD}, with the backbones of the two peptides following the same path along the lateral groove at the dimer interface **(Figures 5E, S6C and S6F)**; this backbone conformation is different from that observed in the BCL6^{BTB-TM}/BCOR^{BBD} complex (Ghetu et al., 2008) and in the complex between BCL6 and the artificial peptide, F1324 (Sakamoto et al., 2017). Structural superposition of the HBP and SMRT^{BBD} peptides reveals an RMSD of 1.09Å **(Figure 5E)**. The side chains of BCL6 residues Arg13, Arg24 and His116 are in the same conformation as found in BCL6^{BTB-TM}/SMRT^{BBD} (Ahmad et al., 2003), adopting a different conformation from that observed in the unliganded BTB domain (Ahmad et al., 2003) and thereby enabling the lateral groove to accommodate the HBP peptide **(Figure S6D)**. In agreement with the BCL6^{BTB-TM}/SMRT^{BBD} structure, serine 11 of the HBP peptide (equivalent to serine 1424 of SMRT) has main chain torsion angles within the alpha-helical region of the Ramachandran plot, causing a kink that enables the peptide to engage with both the upper and lower regions of the BTB domain-binding site **(Figure S6C)**. The main chain and side chain contacts between BCL6 and the ^{1}GRSIHEIPR^{9} moiety of HBP are identical to those observed for the natural SMRT corepressor. The PGGFLCWD moiety of HBP forms a parallel β-sheet with the BTB domain β1-strand, and the register of this β-sheet is most likely constrained by linkage to the ^{1}GRSIHEIPR^{9} sequence. The tryptophan residue contributed by the PGGFLCWD moiety occupies the same location as SMRT E1420 in the BCL6^{BTB-TM}/SMRT^{BBD} structure, and has the same side chain orientation as SMRT E1420 **(Figure S6C and S6E)**; this side chain orientation is different from that found in the BCL6^{BTB-TM}/Apt48 complex, suggesting that linkage to the ^{1}GRSIHEIPR^{9} warhead sequence imposes a steric restriction that promotes the conformational difference **(Figure S6E)**. In the BCL6^{BTB-TM}/HBP complex, the hydrophobic face at the bottom of the BTB domain is predominantly occupied by the L5 side chain of the PGGFLCWD moiety **(Figures S6D and S6E)**. Thus, the alpha carbons of the PGGFLCWD residues of HBP were in the predicted register within the parallel β-sheet, and the side chain orientations differed from those in the BCL6^{BTB-TM}/Apt48 structure; this reflected the stereochemistry of the inverted Apt48 sequence **(Figure S5E)**, and indicated a promiscuity of interactions involving this region.

We have shown that a variety of sequences can interact with lower hydrophobic face of the BTB domain when covalently linked to the ^{1}GRSIHEIPR^{9} peptide that binds to the upper portion of the lateral groove,

and our ITC data has shown that mutation of the BTB domain hydrophobic face can abolish SMRT interactions. This suggests that both portions of the BTB domain binding site may be relevant in determining peptide interactions *in vivo*. We did not determine the affinity of the inverted Apt48 sequence (PGGFLCWD) for the lower portion of the BTB domain, but sought by mutagenesis to examine the relative contribution of HBP residues that bind the two regions.

We altered the sequence of HBP to examine the determinants of its interactions with the upper region of the lateral groove and with the lower hydrophobic face. The PGGFLRRRGRSIHEIPR peptide contains alterations to the sequences that engage the lower hydrophobic face as determined by the structure of the $BCL6^{BTB\text{-}TM}$/HBP complex. This peptide bound $BCL6^{BTB\text{-}DM}$ with a reduced affinity, having a K_d of 64 μM ± 0.18 (N = 1.18 ± 0.13, ΔH = -7.88 kcal/mol ± 0.76, TΔS = -2.15 kcal/mol ± 0.92 and ΔG= -5.73 kcal/mol ± 0.17) **(Figure 5F)**. The peptide PGGFLCWDGRAAHEIPR contains changes in the ^{1}GRSIHEIPR^{9} region that interacts with the upper part of the lateral groove; these alterations abolished the binding of HBP to $BCL6^{BTB\text{-}DM}$ **(Figure 5G),** confirming the importance of the upper portion of the lateral groove in determining the affinity of interactions (Ghetu et al., 2008). We conclude that both regions of the HBP peptide contribute to its high-affinity interaction with the BTB domain, with the GRSIHEIPR sequence being the most important.

Apt48 interacts with the heterodimeric MIZ1/BCL6 BTB domain

BCL6 forms a heterodimeric BTB domain complex with the BTB domain transcription factor, MIZ1, leading to the repression of MIZ1-target genes in DLBCL (Phan et al., 2005). It is therefore relevant to determine whether BCL6-directed therapeutic inhibitors may also interact with the heterodimeric MIZ1/BCL6 BTB domain. We previously solved the structure of the heterodimeric MIZ1/BCL6 BTB domain as a tethered dimer (Stead and Wright, 2014), and showed that its overall organisation resembles that of the BCL6 BTB domain dimer (Stead and Wright, 2014). Although the N-terminus of the MIZ1 BTB domain naturally lacks sequences that form a β1-strand, its β5-strand interacts with β1 of the BCL6 BTB domain in the domain-swapped heterodimer; the structural organisation of the lower part of the heterodimeric BTB domain is thus not symmetrical **(Figure 6A)**. Structural superposition would predict that the Apt48 peptide could interact with the β1-strand and hinge region of the BCL6 moiety on one side of the heterodimeric BTB domain **(Figure 6A)**. We therefore determined whether the Apt48 peptide binds to the ^{15}N-labelled MIZ1/BCL6 heterodimeric BTB domain using ^{1}H-^{15}N TROSY HSQC.

The spectra of the MIZ1/BCL6 heterodimeric BTB domain demonstrated well-dispersed resonances of equal intensities, indicating a compact globular unit. Although the resonances were not assigned, addition of the Apt48 peptide demonstrated clear resonance shift changes of a similar magnitude to those observed upon binding of Apt48 to $BCL6^{BTB\text{-}TM}$, suggesting that Apt48 interacts with the heterodimeric MIZ1/BCL6 BTB

domain **(Figure 6B)**. We therefore expect that, in the context of the MIZ1/BCL6 heterodimer, the BCL6 chain donates the Apt48 binding site to MIZ1.

DISCUSSION

The binding site of the BCL6 BTB domain is a versatile interaction interface that accommodates diverse sequences of transcriptional corepressors and artificial peptides. Our data suggest that this region may conceptually be divided into two portions that can each bind short peptides with low affinity; the high affinity interaction of longer peptides and natural corepressors requires the simultaneous engagement of both regions. The "upper" part comprises the lateral groove and binds short peptides such as the SMRT-derived GRSIHEIPR, whereas the lower portion engages sequences such as Apt48, with high-affinity binding being achieved by the joining of the two. This concept is supported by observations from the unbiased screening strategy of Sakamoto et al (Sakamoto et al., 2017), in which the high-affinity-binding peptide, F1324, was derived by joining discrete consensus sequences that interact with each of the two portions of the BTB domain. A >1000-fold reduction in the binding affinity of F1324 was observed upon removal of its three N-terminal residues that interact with the lower hydrophobic face, further emphasising the importance of this region (Sakamoto et al., 2017). Although the lower hydrophobic face of the BTB domain had not previously been emphasised in corepressor binding studies, its relevance is supported by the alanine-scanning mutagenesis of SMRT and BCOR (Ghetu et al., 2008); binding was abolished by the mutation of corepressor residues that interact with this region, particularly showing the importance of residues that interact at the hinge region between the β1-strand and α1. Conversely, the interaction of SMRT with the BTB domain may be abolished by mutation of BCL6 residues in either the upper lateral groove portion (N21K)(Ahmad et al., 2003), or in the lower portion (I9 or F11) as reported here.

The extended binding site of the BCL6 BTB domain may have evolved to ensure the specificity of its interactions with transcriptional corepressors, with the simultaneous engagement of the two regions being required both for high-affinity binding and to prevent promiscuous interactions. Natural corepressors interact with the upper portion of the lateral groove in more than one conformation, and the requirement to simultaneously engage with the lower portion of the BTB domain might provide a mechanism to prevent unwanted interactions with intrinsically disordered proteins in the crowded environment of the nuclear bodies (reviewed in (Uversky, 2017)) where BCL6 resides *in vivo* (Dhordain et al., 1995). Although the interactions with the lower binding site show less sequence specificity, it appears important that this site is occupied. The interaction of intrinsically disordered proteins with their partners frequently involves multiple short linear sequences, with avidity effects leading to high affinity interaction (reviewed in (Wright

and Dyson, 2015)) and the binding to target proteins may involve both conformational selection and induced fit mechanisms (reviewed in (Latysheva et al., 2015)). The sequence requirements of peptides that interact with the BTB domain have not been exhaustively analysed, and it is feasible that these must be compatible with specific structural conformations capable of spanning both the upper and lower regions of the binding site.

Previous approaches for the therapeutic targeting of BCL6 have focussed on inhibitors that bind the aromatic pocket located at the upper part of the lateral groove. Our finding that the known inhibitor sequence, Apt48, interacts with the lower portion of the BTB domain suggests the feasibility of new approaches that specifically target this region. Such approaches would also target the heterodimeric MIZ1/BCL6 BTB domain, which is not predicted to bind known small molecule inhibitors that interact with the upper lateral groove (Cerchietti et al., 2010). Although the Apt48 peptide interacts with the BCL6 BTB domain with low affinity as assessed by NMR, and we were unable to measure the interaction under the experimental conditions of ITC, it has been noted that the aptamer inhibits BCL6 when present at low concentrations in the DLBCL cell line Ramos (Chattopadhyay et al., 2006). Other low-affinity inhibitors of BCL6 include the small molecule, 79-6 (Kd ~138 μM) (Cerchietti et al., 2010) and the ansamycin antibiotic, rifabutin (Kd ~1 mM)(Evans et al., 2014), each of which target the upper portion of the lateral groove. It is also notable that the biological mechanisms of BCL6 inhibitors have not always been as predicted, and some small molecules that target the lateral groove act by unexpectedly enhancing BCL6 protein degradation (Kerres et al., 2017; Bellenie et al., 2020; Slabicki et al., 2020). Such phenomena could explain the effectiveness of weak-binding inhibitors *in vivo*, and the biological mechanisms of inhibition by Apt48 and other compounds thus needs further investigation. The interactions of the lower hydrophobic face will also be relevant in the design of peptide inhibitors that target the BTB domain. Although previously described peptide inhibitors have been designed to target the upper portion of the lateral groove, the fortuitous interaction of the nuclear-targeting TAT sequences included in these peptides may have contributed to their efficacy. In addition to the treatment of DLBCL, BCL6 inhibitors may have applications in other haematological malignancies, in solid cancers (reviewed in (Cardenas et al., 2017), and in treating chronic graft-versus-host disease that is driven by BCL6 (Paz et al., 2019). Our characterisation of the interaction between Apt48 and BCL6 thus provides crucial information for the design of new families of peptide and small molecule inhibitors.

ACKNOWLEDGMENTS

We thank Diamond Light Source (proposal MX15378) and ESRF (proposal MX1988) for beamtime, and the staff of Diamond beamline I24 and ESRF beamline ID29 for X-ray data collection. We gratefully

acknowledge the Kay Kendall Leukaemia Fund for funding this work (award KKLF1047), and the Wellcome Trust (094232) for funding the NMR instrumentation.

AUTHOR CONTRIBUTIONS

TZ and SCW conceived the project, designed experiments, analysed data and wrote the manuscript. TZ additionally performed ITC, NMR and crystallography, and APK performed NMR and analysed the NMR data.

DECLARATION OF INTERESTS

The authors declare no competing interests.

MAIN FIGURE TITLES AND LEGENDS

Figure 1

Apt48 binds a lower hydrophobic face of the BCL6 BTB domain

A) ^{1}H-^{15}N TROSY HSQC spectra of $BCL6^{BTB\text{-}TM}$ in the absence (blue) and presence (red) of an 8-fold molar excess of Apt48 peptide. Chemical shift perturbations on I9, Q10, G55 and E115 are indicated. Full spectra are shown in Figure S2B.

B) Surface display of the dimeric BCL6 BTB domain (PDB entry 1r29; Ahmad et al., 2003). The A and B chains are depicted in brown and light blue respectively, and residues that have a chemical shift change greater than 2σ (Figure S2B) upon Apt48 binding are shown in dark blue. Residues of the B chain are indicated with a prime; residues G55, L56, E115, V117 and L25' are hidden from view on the opposite face of the BTB dimer. See also Figure S1.

Figure 2

Structure of the $BCL6^{BTB\text{-}TM}$/Apt48 complex

A) Crystal structure of the $BCL6^{BTB\text{-}TM}$/Apt48 complex solved to 1.63Å resolution. BCL6 chains A and B are depicted in brown and light blue respectively, and the Apt48 peptide in green. Secondary structure

elements of the B chain are indicated with a prime. A simulated annealing composite omit map of the Apt48 peptide is shown in Figure S3A, and details of contacts are shown in Figures S3B, S3C and S3D.

B) Close-up view of the interface between the Apt48 peptide and the BTB domain. Residues of Apt48 are italicised in green.

C) ^{1}H-^{15}N TROSY HSQC spectra of BCL6$^{BTB\text{-}TM}$ in the absence (blue) and presence (red) of mutated Apt48 peptides: Apt48P2R, Apt48ΔN and Apt48W8R. Peptides were at an 8-fold molar excess, except for Apt48ΔN, where only a 3-fold molar excess was possible due to solubility.

Figure 3

The hydrophobic face of the BCL6 BTB domain is required for interaction with SMRT

ITC titrations of the SMRT^{BBD} peptide into BCL6 BTB domain mutants. See also Figure S4.

Figure 4

The ^{1}GRSIHEIPR^{9} sequence directs peptide recruitment to the lateral groove

A) ITC titration of the ^{1}GRSIHEIPR^{9} peptide into BCL6$^{BTB\text{-}DM}$.

B) Interaction of the ^{1}GRSIHEIPR^{9} peptide with BCL6$^{BTB\text{-}TM}$ as measured by ^{1}H-^{15}N TROSY HSQC (see also Figures S5A and S5B). The surface display (PDB entry 1r29; Ahmad et al., 2003) depicts the A and B chains in brown and light blue respectively; BCL6 residues that have a chemical shift change greater than 2σ or broadening upon ^{1}GRSIHEIPR^{9} binding are shown in dark blue. Residues that are not shown are either buried or located on the opposite face of the BTB dimer.

C) ITC titration of the TAT-GRSIHEIPR peptide into BCL6$^{BTB\text{-}DM}$.

Figure 5

A hybrid BTB-binding peptide (HBP) interacts with the lateral groove

A) Sequences of the Apt48ΔN and truncated SMRT^{BBD} peptides, together with a sequence alignment of peptides that bind to the BCL6 BTB domain. Green shading indicates residues that interact with the hydrophobic face that encompasses the β1-strand, as indicated from crystal structures; red shading indicates residues that interact with the upper part of the lateral groove.

B) ITC titration of the HBP peptide into BCL6$^{BTB\text{-}DM}$.

C) Crystal structure of the BCL6$^{BTB\text{-}TM}$/HBP complex solved to 2.09Å. BCL6 chains A and B are shown in brown and light blue respectively. The part of the peptide that interacts with the hydrophobic face

encompassing the β1-strand is shown in green, and the part that interacts with the upper portion of the lateral groove is in red. A simulated annealing omit map of the HBP peptide is shown in Figure S6B.

D) Close-up view of HBP peptide interactions with the BTB domain β1-strand. Residues of HBP are italicised in green. Details of contacts are shown in Figure S6D and S6F.

E) Structural superposition of peptides that interact with the BCL6 BTB domain. Crystal structures of $BCL6^{BTB\text{-}TM}$/$SMRT^{BBD}$ (PDB entry 1r2b; Ahmad et al., 2003), $BCL6^{BTB\text{-}TM}$/$BCOR^{BBD}$ (PDB entry 3bim chains A, B, I, J; Ghetu et al., 2008), $BCL6^{BTB}$/F1324 (PDB entry 5h7g; Sakamoto et al., 2017) and $BCL6^{BTB\text{-}TM}$/HBP were superposed by structural alignment of the BTB chains; the backbone conformations of the corresponding peptides are shown. See also Figures S6C and S6E.

F) ITC titration of the HBP mutant peptide, PGGFLRRRGRSIHEIPR, into $BCL6^{BTB\text{-}DM}$.

G) ITC titration of the HBP mutant peptide, PGGFLCWDGRAAHEIPR, into $BCL6^{BTB\text{-}DM}$.

Figure 6

Apt48 interacts with the heterodimeric MIZ1/BCL6 BTB domain

A) Model of the heterodimeric MIZ/BCL6 BTB domain in complex with the Apt48 peptide, generated by superposition of the $BCL6^{BTB\text{-}TM}$/Apt48 structure onto the MIZ1/BCL6 BTB domain (PDB entry 4u2m chain A; Stead et al., 2014). BCL6 residues are depicted in brown, and MIZ residues in light blue. α1 and β1 of the BCL6 chain, and β5 and α6 of MIZ1 are labelled.

B) ^{1}H-^{15}N TROSY HSQC spectra of the MIZ1/BCL6 BTB domain in the absence (blue) and presence (red) of an 8-fold molar excess of Apt48 peptide.

MAIN TABLES AND LEGENDS

Table 1 Crystallographic statistics

	$BCL6^{BTB-TM}$/Apt48 (PDB:6tbt)	$BCL6^{BTB-TM}$/HBP (PDB:6tcj)
Diffraction data		
Beamline	I24-Diamond	ID29-ESRF
Wavelength (Å)	0.9686	0.9793
Resolution range (Å)	78.20-1.63 (1.67-1.63)	47.25-2.13 (2.18-2.13)
Space group	P 31 2 1	P 1 21 1
Unit Cell		
a,b,c (Å)	65.63, 65.63, 156.40	39.66, 47.30, 76.37
α,β,γ (°)	90, 90, 120	90.0, 94.34, 90.0
Unique reflections	49659 (3587)	15991 (1171)
Completeness (%)	100 (100)	99.8 (100)
Multiplicity	19.4 (19.90)	3.30 (3.10)
CC1/2	0.998 (0.554)	0.981 (0.386)
I/σ(I)	15.90 (1.9)	4.3 (1.0)
$R_{merge\ (I)}$	0.112 (1.75)	0.183 (1.268)
R_{pim}	0.037 (0.57)	0.172 (1.187)
Refinement		
R_{work} (%)	15.30	19.93
R_{free} (%)	17.80	24.95
Number of atoms	2,402	2,354
Macromolecule	2,090	2,261
Solvent	298	92
Other	14	1
RMSD bonds (Å)	0.009	0.0083
RMSD angles (°)	1.33	1.27
Ramachandran favoured (%)	99.20	97.43
Ramachandran allowed (%)	0.8	2.57

Data and reduction statistics, with values of the highest resolution shell shown in parentheses. R free is calculated from 5% of reflections isolated from refinement for cross-validation. Geometry statistics were calculated using Molprobity (Chen et al., 2010). TLS groups included each chain from each respective structure.

STAR*METHODS

KEY RESOURCES TABLE

RESOURCE AVAILABILITY

Lead Contact

Further information and requests for resources and reagents should be directed to and will be fulfilled by the Lead Contact, Stephanie Wright (s.c.wright@leeds.ac.uk)

Materials Availability

Materials generated in this study are available upon request to the Lead Contact.

Data and Code Availability

- Coordinates and structure factors have been deposited at the RCSB Protein Data Bank and are publicly available as of the date of publication. Accession numbers are listed in the Key Resources Table.
- This paper does not report original code.
- Any additional information required to reanalyze the data reported in this paper is available from the Lead Contact upon request.

EXPERIMENTAL MODEL AND SUBJECT DETAILS

Bacterial cell culture

Cloning was carried out in *Escherichia coli* Stellar^{TM} cells, and cells transformed with plasmid were grown in TB media containing 34 μg/ml kanamycin at 310K. Protein expression was carried out in *Escherichia coli* BL21 (DE3) pLysS cells. 1L cultures were grown shaking at 200 rpm, 310K to an OD_{600} of 0.6, cooled to 291K, and recombinant protein then induced by growth for a further 18 hours at 291K in the presence of 500 μM IPTG. Proteins for NMR spectroscopy were prepared in 2M9 medium supplemented with ammonium-^{15}N chloride (Sigma).

METHOD DETAILS

Peptides

Peptides were synthesised by GL Biochem Shanghai Ltd. Sequences were: ^{1}GPHGPRDWCLFGGP^{14} (Apt48), ^{1}GRHGPRDWCLFGGP^{14} (Apt48P2R), ^{1}GPHGPRDRCLFGGP^{14} (Apt48W8R), ^{7}DWCLFGGP^{14} (Apt48ΔN), ^{1}PGGFLCWDGRSIHEIPR^{17} (HBP), ^{1}LVATVKEAGRSIHEIPR^{17} (SMRT^{BBD}), ^{1}GRSIHEIPR^{9} ("truncated" SMRT^{BBD}), YGRKKRRQRRRGGRSIHEIPR (TAT-GRSIHEIPR), PGGFLRRRGRSIHEIPR (mutated HBP) and PGGFLCWDGRAAHEIPR (mutated HBP). Peptides were dissolved in appropriate buffers for ITC, NMR or crystallography, and the pH adjusted to experimental conditions prior to use.

Plasmids

The human BCL6 BTB domain (residues 6 - 129; UniProt accession P41182) and the Miz1/BCL6 tethered heterodimer (Stead and Wright, 2014) were cloned into a modified pET28a vector encoding an N-terminal hexa-histidine-MBP tag using ligation-independent cloning (Infusion, Clontech). Point mutations were generated by PCR using Phusion High-Fidelity DNA polymerase (Thermo Scientific). The BCL6 BTB triple mutant (BCL6$^{BTB\text{-}TM}$) contained the mutations C8Q, C67R and C84N as previously used for crystallographic studies (Ahmad et al., 2003). The BCL6 BTB double mutant (BCL6$^{BTB\text{-}DM}$) contained the mutations C67R and C84N. The Miz1/BCL6 heterodimer contained the wild-type BCL6 sequence. All constructs were verified by DNA sequencing (GENEWIZ).

Protein expression and purification

Cells were harvested by centrifugation at 11,000 *g* and resuspended in 20 mM Na_2HPO_4, 500 mM NaCl, 40 mM imidazole and 3 mM β-mercaptoethanol pH 7.4. Bovine Deoxyribonuclease 1 (Sigma) and Protease Inhibitor Cocktail VII (Merck) were added, and the cells were lysed at 30K psi using a cell disruptor (Constant Systems). The lysate was clarified by centrifugation at 39,000 *g* for 45 minutes, and proteins purified via Immobilised Metal Affinity Chromatography (IMAC) using a 5ml His-Trap HP column (GE Healthcare). The N-terminal His-MBP tag was removed by cleavage with HR3C protease, and the protein further purified by size-exclusion chromatography on a Superdex 75 HiLoad 26/60 column (GE Healthcare).

NMR spectroscopy

NMR spectra were collected on a 750 MHz Bruker Avance spectrometer equipped with a cryoprobe. ^{1}H-^{15}N TROSY data for BCL6$^{BTB\text{-}TM}$ (400 μM) were collected at 298K in 20 mM Na_2HPO_4 pH 6.8, 300 mM NaCl and 3 mM β-mercaptoethanol. Data for MIZ1/BCL6^{BTB} (400 μM) were collected in 20 mM HEPES pH 7.5, 150 mM NaCl and 3 mM β-mercaptoethanol. The backbone assignment for BCL6$^{BTB\text{-}TM}$ was transferred from the deposited BMRB entry 27079 (Lin et al., 2018) using CCPN analysis (Vranken et al., 2005).

Isothermal titration calorimetry

Data were collected on a MicroCal iTC200 calorimeter (Malvern Panalytical) at 298 K in 20 mM Na_2HPO_4 pH 6.8, 300 mM NaCl and 1 mM TCEP. The sample cell contained 200µl 83 µM $BCL6^{BTB}$ protein, and experiments consisted of 25 injections of a 15-fold molar excess of peptide. Data were fit assuming a single site model using Origin Pro, where K_d= 1/Ka. All data were collected in duplicate runs, and thermodynamic analysis shows averaged statistics from duplicate runs.

X-ray crystallography

$BCL6^{BTB-TM}$ protein was concentrated to 300 µM (monomer) in 20 mM HEPES pH 7.5, 300 mM NaCl and 3mM β-mercaptoethanol, and mixed with a 12-fold molar excess of the Apt48 peptide or with a 4-fold molar excess of the hybrid BBD (HBP) peptide. Sitting-drop sparse matrix crystallisation screening was performed using a Mosquito solution handling robot (TTP Labtech) with 400 nl drops and a 1:1 protein:precipitant ratio.

Crystals of the $BCL6^{BTB-TM}$ /Apt48 complex were obtained in 2.4 M NaCl, 0.1 M Tris pH 7, 0.2 M $MgCl_2$ at 291K, and were vitrified in liquid nitrogen using mother liquor supplemented with 25% glycerol. Data were collected on beamline I24 (Diamond Light Source, Oxford) using a non-overlapping 0.2^o oscillation width and a 360^o rotation. Data reduction and scaling was done with *XDS* (Kabsch, 2010) and *AIMLESS* using the *xia*2 pipeline (Winter, 2010). Analysis of the cumulative intensity distribution and of the intensity moments using *Phenix Xtriage* (Adams et al., 2010) indicated that the data were twinned. Further analysis of the data revealed the presence of a merohedral twin operator and the corresponding fractions of 0.55 h, k, l and 0.44 -h,-k, l with a Robs for twin-related reflections of 0.065 in the space group $P3_121$. The structure was solved by molecular replacement using *Phaser* (McCoy et al., 2007) with the template model 1r2b (Ahmad et al, 2003). High-quality electron density for the Apt48 peptide was clearly visible in the F_O-F_C map post molecular replacement (Figure S3A). The models underwent iterative rounds of twinned refinement in *REFMAC* (Murshudov et al., 2011) and PDB-REDO (Joosten et al., 2012). Models were built using *Coot* (Emsley et al., 2010).

Crystals of the $BCL6^{BTB-TM}$/HBP complex were obtained in 9.9% (v/v) MPD, 2.64% (w/v), PEG 8000 0.5 M NaCl, 0.1M Tris pH 8.5 at 291K, and were vitrified in liquid nitrogen using mother liquor supplemented with 25% glycerol. Data were collected on beamline ID29 ESRF using a 0.1^o oscillation width and 180^o rotation. Data reduction and scaling was done with *XIA2DIALS* and the structure was solved by molecular replacement using *Phaser* (Mc Coy *et al*., 2007) with the search model 1r2b (Ahmad et al, 2003) in space

group $P12_11$. Refinement was performed using REFMAC (Murshudov et al., 2011) and PDB-REDO (Joosten et al., 2012).

Integration and refinement statistics of the $BCL6^{BTB-TM}$/Apt48 and $BCL6^{BTB-TM}$/HBP complexes are shown in Table 1. Atomic coordinates and structure factors were deposited to the PDB with the accession codes 6tbt and 6tcj. Illustrations of protein structures were prepared using PyMol Molecular Graphics System, Schrödinger, LLC. Figures of protein interactions were prepared using LigPlot (Laskowski and Swindells, 2011).

QUANTIFICATION AND STATISTICAL ANALYSIS

The processing and analysis of X-ray data were carried out as described and referenced in the Method Details section. Molecular replacement used *Phaser* (CCP4 suite), and refinement was carried out using both the PDB-REDO pipeline and *REFMAC* (CCP4 suite), with iterative model building in *Coot* (CCP4 suite), as detailed in the Key Resources Table. ITC data are the mean of two independent runs; the means and standard deviations for each experiment are indicated in the Results.

REFERENCES

Adams, P.D., Afonine, P.V., Bunkóczi, G., Chen, V.B., Davis, I.W., Echols, N., Headd, J.J., Hung, L.W., Kapral, G.J., Grosse-Kunstleve, R.W., et al. (2010). PHENIX: a comprehensive Python-based system for macromolecular structure solution. Acta Crystallogr. D Biol. Crystallogr., *66*, 213-221.

Ahmad, K.F., Melnick, A., Lax, S., Bouchard, D., Liu, J., Kiang, C.L., Mayer, S., Takahashi, S., Licht, J.D., and Privé, G.G. (2003). Mechanism of SMRT corepressor recruitment by the BCL6 BTB domain. Mol. Cell, *12*, 1551-1564.

Ai, Y., Hwang, L., MacKerell Jr., A.D., Melnick, A., and Xue, F. (2021). Progress toward B-cell lymphoma 6 BTB domain inhibitors for the treatment of diffuse large B-cell lymphoma and beyond. J. Med. Chem., *64,* 4333-4358.

Baron, B.W., Nucifora, G., McCabe, N., Espinosa, R., 3rd, Le Beau, M.M., and McKeithan, T.W. (1993). Identification of the gene associated with the recurring chromosomal translocations t(3;14)(q27;q32) and t(3;22)(q27;q11) in B-cell lymphomas. Proc. Natl. Acad. Sci. U. S. A., *90*, 5262-5266.

Bellenie, B.R., Cheung, K.J., Varela, A., Pierrat, O.A., Collie, G.W., Box, G.M., Bright, M.D., Gowan, S., Hayes, A., Rodrigues, M.J. et al. (2020). Achieving *in vivo* target depletion through the discovery and optimization of benzimidazolone BCL6 degraders. J. Med. Chem., *63,* 4047-4068.

Basso, K., and Dalla-Favera, R. (2010). BCL6: master regulator of the germinal center reaction and key oncogene in B cell lymphomagenesis. Adv. Immunol., *105*, 193-210.

Basso, K., and Dalla-Favera, R. (2012). Roles of BCL6 in normal and transformed germinal center B cells. Immunol. Rev., *247*, 172-183.

Buchan, D.W.A., and Jones, D.T. (2019). The PSIPRED Protein Analysis Workbench: 20 years on. Nucleic Acids Res*., 47*, W402-w407.

Cardenas, M.G., Oswald, E., Yu, W., Xue, F., MacKerell, A.D. Jr., and Melnick, A.M. (2017). The Expanding Role of the BCL6 Oncoprotein as a Cancer Therapeutic Target. Clin. Cancer Res*., 23*, 885-893.

Cardenas, M.G., Yu, W., Beguelin, W., Teater, M.R., Geng, H., Goldstein, R.L., Oswald, E., Hatzi, K., Yang S,N., Cohen, J., et al. (2016). Rationally designed BCL6 inhibitors target activated B cell diffuse large B cell lymphoma. J. Clin. Invest*., 126*, 3351-3362.

Cerchietti, L.C., Ghetu, A.F., Zhu, X., Da Silva, G.F., Zhong, S., Matthews, M., Bunting, K.L., Polo, J.M., Farès, C., Arrowsmith, C.H., et al. (2010). A small-molecule inhibitor of BCL6 kills DLBCL cells in vitro and in vivo. Cancer Cell*, 17*, 400-411.

Cerchietti, L.C., Yang, S.N., Shaknovich, R., Hatzi, K., Polo, J.M., Chadburn, A., Dowdy, S.F., and Melnick, A. (2009). A peptomimetic inhibitor of BCL6 with potent antilymphoma effects in vitro and in vivo. Blood*, 113*, 3397-3405.

Chattopadhyay, A., Tate, S.A., Beswick, R.W., Wagner, S.D., and Ko Ferrigno, P. (2006). A peptide aptamer to antagonize BCL-6 function. Oncogene*, 25*, 2223-2233.

Chen, V.B., Arendall, W.B. 3rd, Headd, J.J., Keedy, D.A., Immormino, R.M., Kapral, G.J., Murray, L.W., Richardson, J.S., and Richardson, D.C. (2010). MolProbity: all-atom structure validation for macromolecular crystallography. Acta Crystallogr. D Biol. Crystallogr*., 66*, 12-21.

Cheng, H., Linhares, B.M., Yu, W., Cardenas, M.G., Ai, Y., Jiang, W., Winkler, A., Cohen, S., Melnick, A., MacKerell, A. Jr., et al. (2018). Identification of Thiourea-Based Inhibitors of the B-Cell Lymphoma 6 BTB Domain via NMR-Based Fragment Screening and Computer-Aided Drug Design. J. Med. Chem*., 61*, 7573-7588.

Dent, A.L., Shaffer, A.L., Yu, X., Allman, D., and Staudt, L.M. (1997). Control of inflammation, cytokine expression, and germinal center formation by BCL-6. Science*, 276*, 589-592.

Dhordain, P., Albagli, O., Ansieau, S., Koken, M.H., Deweindt, C., Quief, S., Lantoine, D., Leutz, A., Kerckaert, J.P., and Leprince, D. (1995). The BTB/POZ domain targets the LAZ3/BCL6 oncoprotein to nuclear dots and mediates homomerisation in vivo. Oncogene*, 11*, 2689-2697.

Dhordain, P., Albagli, O., Lin, R. J., Ansieau, S., Quief, S., Leutz, A., Kerckaert, J.P., Evans, R.M., and Leprince, D. (1997). Corepressor SMRT binds the BTB/POZ repressing domain of the LAZ3/BCL6 oncoprotein. Proc. Natl. Acad. Sci. U. S. A*., 94*, 10762-10767.

Emsley, P., Lohkamp, B., Scott, W.G., and Cowtan, K. (2010). Features and development of Coot. Acta Crystallogr. D Biol. Crystallogr*., 66*, 486-501.

Evans, S.E., Goult, B.T., Fairall, L., Jamieson, A.G., Ko Ferrigno, P., Ford, R., Schwabe, J.W., and Wagner, S.D. (2014). The ansamycin antibiotic, rifamycin SV, inhibits BCL6 transcriptional repression and forms a complex with the BCL6-BTB/POZ domain. PLoS One*, 9*, e90889.

Ghetu, A.F., Corcoran, C.M., Cerchietti, L., Bardwell, V.J., Melnick, A., and Prive, G.G. (2008). Structure of a BCOR corepressor peptide in complex with the BCL6 BTB domain dimer. Mol. Cell*, 29*, 384-391.

Hatzi, K., Jiang Y., Huang, C., Garrett-Bakelman, F., Gearhart, M.D., Giannopoulou, E.G., Zumbo, P., Kirouac, K., Bhaskara, S., Polo J.M., et al. (2013). A hybrid mechanism of action for BCL6 in B cells defined by formation of functionally distinct complexes at enhancers and promoters. Cell Rep*., 4*, 578-588.

Hatzi, K., and Melnick, A. (2014). Breaking bad in the germinal center: how deregulation of BCL6 contributes to lymphomagenesis. Trends Mol. Med*., 20*, 343-352.

Huang, C., Gonzalez, D.G., Cote, C.M., Jiang, Y., Hatzi, K., Teater, M., Dai, K., Hla, T., Haberman, A.M., and Melnick A. (2014). The BCL6 RD2 domain governs commitment of activated B cells to form germinal centers. Cell Rep*., 8*, 1497-1508.

Huang, C., Hatzi, K., and Melnick, A. (2013). Lineage-specific functions of Bcl-6 in immunity and inflammation are mediated by distinct biochemical mechanisms. Nat. Immunol*., 14*, 380-388.

Huynh, K.D., and Bardwell, V.J. (1998). The BCL-6 POZ domain and other POZ domains interact with the co-repressors N-CoR and SMRT. Oncogene*, 17*, 2473-2484.

Huynh, K.D., Fischle, W., Verdin, E., and Bardwell, V.J. (2000). BCoR, a novel corepressor involved in BCL-6 repression. Genes Dev*., 14*, 1810-1823.

Jones, D.T. (1999). Protein secondary structure prediction based on position-specific scoring matrices. J. Mol. Biol*., 292*, 195-202.

Joosten, R.P., Joosten, K., Murshudov, G.N., and Perrakis, A. (2012). PDB_REDO: constructive validation, more than just looking for errors. Acta Crystallogr. D Biol. Crystallogr*., 68*, 484-496.

Joosten, R.P., Long, F., Murshudov, G.N., and Perrakis A. (2014). The PDB_REDO server for macromolecular structure model optimization. IUCrJ, *1,* 213-220.

Kabsch, W. (2010). XDS. Acta Crystallogr. D Biol. Crystallogr*., 66*, 125-132.

Kamada, Y., Sakai, N., Sogabe, S., Ida, K., Oki, H., Sakamoto, K,. Lane, W., Snell, G., Iida, M., Imaeda, Y., et al. (2017). Discovery of a B-Cell Lymphoma 6 Protein-Protein Interaction Inhibitor by a Biophysics-Driven Fragment-Based Approach. J. Med. Chem*., 60*, 4358-4368.

Kerckaert, J.P., Deweindt, C., Tilly, H., Quief, S., Lecocq, G., and Bastard, C. (1993). LAZ3, a novel zinc-finger encoding gene, is disrupted by recurring chromosome 3q27 translocations in human lymphomas. Nat. Genet*., 5*, 66-70.

Kerfoot, S.M., Yaari, G., Patel, J.R., Johnson, K.L., Gonzalez, D G., Kleinstein, S.H., and Haberman, A.M. (2011). Germinal center B cell and T follicular helper cell development initiates in the interfollicular zone. Immunity*, 34*, 947-960.

Kerres, N., Steurer, S., Schlager, S., Bader, G., Berger, H., Caligiuri, M., Dank, C., Engen, J.R., Ettmayer, P., Fischerauer, B., et al. (2017). Chemically Induced Degradation of the Oncogenic Transcription Factor BCL6. Cell Rep*., 20*, 2860-2875.

Kitano, M., Moriyama, S., Ando, Y., Hikida, M., Mori, Y., Kurosaki, T., and Okada, T. (2011). Bcl6 protein expression shapes pre-germinal center B cell dynamics and follicular helper T cell heterogeneity. Immunity*, 34*, 961-972.

Klein, U., and Dalla-Favera, R. (2008). Germinal centres: role in B-cell physiology and malignancy. Nat. Rev. Immunol*., 8*, 22-33.

Laskowski, R. A., and Swindells, M.B. (2011) LigPlot+: multiple ligand-protein interaction diagrams for drug discovery. J. Chem. Inf. Model., *51,* 2778-2786.

Latysheva, N.S., Flock, T., Weatheritt, R.J., Chavali, S., and Babu, M.M. (2015). How do disordered regions achieve comparable functions to structured domains? Protein Sci*., 24*, 909-922.

Liebschner, D., Afonine, P.V., Baker, M.L., Bunkóczi, G., Chen, V.B., Croll, T.I., Hintze, B., Hung, L.W., Jain, S., McCoy, A.J., et al. (2019). Macromolecular structure determination using X-rays, neutrons and electrons: recent developments in Phenix. Acta Crystallogr. D Biol. Crystallogr., *75,* 861-877.

Lin, L.Y., Evans, S.E., Fairall, L., Schwabe, J.W.R., Wagner, S.D., and Muskett, F.W. (2018). Backbone resonance assignment of the BCL6-BTB/POZ domain. Biomol NMR Assign*, 12*, 47-50.

McCoy, A.J., Grosse-Kunstleve, R.W., Adams, P.D., Winn, M.D., Storoni, L.C., and Read, R.J. (2007). Phaser crystallographic software. J Appl Crystallogr*, 40*, 658-674.

Merkel, J.S., Sturtevant, J.M. and Regan, L. (1999). Sidechain interactions in parallel β sheets: the energetics of cross-strand pairings. Structure, *7*, 1333-1343.

Murshudov, G.N., Skubak, P., Lebedev, A.A., Pannu, N.S., Steiner, R.A., Nicholls, R.A., Winn, M.D., Long, F., and Vagin, A.A. (2011). REFMAC5 for the refinement of macromolecular crystal structures. Acta Crystallogr. D Biol. Crystallogr*., 67*, 355-367.

Nurieva, R.I., Chung, Y., Martinez, G.J., Yang, X.O., Tanaka, S., Matskevitch, T.D., Wang, Y.H., and Dong, C. (2009). Bcl6 mediates the development of T follicular helper cells. Science*, 325*, 1001-1005.

Paz, K., Flynn, R., Du, J., Qi, J., Luznik, L., Maillard, I., MacDonald, K.P., Hill, G.R., Serody, J.S., Murphy, W.J., et al. (2019). Small-molecule BCL6 inhibitor effectively treats mice with nonsclerodermatous chronic graft-versus-host disease. Blood*, 133*, 94-99.

Phan, R.T., Saito, M., Basso, K., Niu, H., and Dalla-Favera, R. (2005). BCL6 interacts with the transcription factor Miz-1 to suppress the cyclin-dependent kinase inhibitor p21 and cell cycle arrest in germinal center B cells. Nat. Immunol*., 6*, 1054-1060.

Polo, J.M., Dell'Oso, T., Ranuncolo, S.M., Cerchietti, L., Beck, D., Da Silva, G.F., Prive, G.G., Licht, J.D., and Melnick, A. (2004). Specific peptide interference reveals BCL6 transcriptional and oncogenic mechanisms in B-cell lymphoma cells. Nat. Med*., 10*, 1329-1335.

Saito, M., Novak, U., Piovan, E., Basso, K., Sumazin, P., Schneider, C., Crespo, M., Shen, Q., Bhagat, G., Califano, A., et al. (2009). BCL6 suppression of BCL2 via Miz1 and its disruption in diffuse large B cell lymphoma. Proc. Natl. Acad. Sci. U. S. A*., 106*, 11294-11299.

Sakamoto, K., Sogabe, S., Kamada, Y., Sakai, N., Asano, K., Yoshimatsu, M., Ida, K., Imaeda, Y., and Sakamoto, J. I. (2017). Discovery of high-affinity BCL6-binding peptide and its structure-activity relationship. Biochem. Biophys. Res. Commun*., 482*, 310-316.

Seyfert, V.L., Allman, D., He, Y., and Staudt, L.M. (1996). Transcriptional repression by the proto-oncogene BCL-6. Oncogene*, 12*, 2331-2342.

Slabicki, M. Yoon, H., Koeppel, J., Nitsch, L., Roy Burman, S.S., Di Genua, C., Donovan, K.A., Sperling, A.S., Hunkeler, M., Tsai, J.M., et al. (2020). Small-molecule-induced polymerization triggers degradation of BCL6. Nature *588,*164-168.

Skinner, S.P., Fogh, R.H., Boucher, W., Ragan, T.J., Mureddu, L.G., and Vuister, G.W. (2016). CcpNmr AnalysisAssign: a flexible platform for integrated NMR analysis. J. Biomol. NMR, *66*, 111-124.

Stead, M.A., and Wright, S.C. (2014). Structures of heterodimeric POZ domains of Miz1/BCL6 and Miz1/NAC1. Acta Crystallogr F Struct Biol Commun*, 70*, 1591-1596.

Toney, L.M., Cattoretti, G., Graf, J.A., Merghoub, T., Pandolfi, P.P., Dalla-Favera, R., Ye, B.H., and Dent, A.L. (2000). BCL-6 regulates chemokine gene transcription in macrophages. Nat. Immunol*., 1*, 214-220.

Uversky, V.N. (2017). Intrinsically disordered proteins in overcrowded milieu: Membrane-less organelles, phase separation, and intrinsic disorder. Curr. Opin. Struct. Biol*., 44*, 18-30.

Vranken, W.F., Boucher, W., Stevens, T.J., Fogh, R.H., Pajon, A., Llinas, M., Ulrich, E.L., Markley, J.L., Ionides, J., and Laue, E.D. (2005). The CCPN data model for NMR spectroscopy: development of a software pipeline. Proteins*, 59*, 687-696.

Winn, M.D., Ballard, C.C., Cowtan, K.D., Dodson, E.J., Emsley, P., Evans, P.R., Keegan, R.M., Krissinel, E B., Leslie, A.G., McCoy, A., et al. (2011). Overview of the CCP4 suite and current developments. Acta Crystallogr. D. Biol. Crystallogr. *67,* 235-242.

Winter, G. (2010). xia2: an expert system for macromolecular crystallography data reduction. Journal of Applied Crystallography*, 43*, 186-190.

Wong, C.W., and Privalsky, M.L. (1998). Components of the SMRT corepressor complex exhibit distinctive interactions with the POZ domain oncoproteins PLZF, PLZF-RARalpha, and BCL-6. J. Biol. Chem*., 273*, 27695-27702.

Wright, P.E., and Dyson, H.J. (2015). Intrinsically disordered proteins in cellular signalling and regulation. Nat. Rev. Mol. Cell Biol*., 16*, 18-29.

Yasui, T., Yamamoto, T., Sakai, N., Asano, K., Takai, T., Yoshitomi, Y., Davis, M., Takagi, T., Sakamoto, K., Sogabe, S., et al. (2017). Discovery of a novel B-cell lymphoma 6 (BCL6)-corepressor interaction inhibitor by utilizing structure-based drug design. Bioorg. Med. Chem*., 25*, 4876-4886.

Ye, B. H., Cattoretti, G., Shen, Q., Zhang, J., Hawe, N., de Waard, R., Leung, C., Nouri-Shirazi, M., Orazi, A., Chaganti, R.S., et al. (1997). The BCL-6 proto-oncogene controls germinal-centre formation and Th2-type inflammation. Nat. Genet*., 16*, 161-170.

Ye, B.H., Lista, F., Lo Coco, F., Knowles, D.M., Offit, K., Chaganti, R.S., and Dalla-Favera, R. (1993). Alterations of a zinc finger-encoding gene, BCL-6, in diffuse large-cell lymphoma. Science*, 262*, 747-750.

Zacharchenko, T., and Wright, S.C. (2021). Functionalization of the BCL6 BTB domain into a noncovalent crystallization chaperone. IUCrJ, *8*, 154-160.

Figure 1

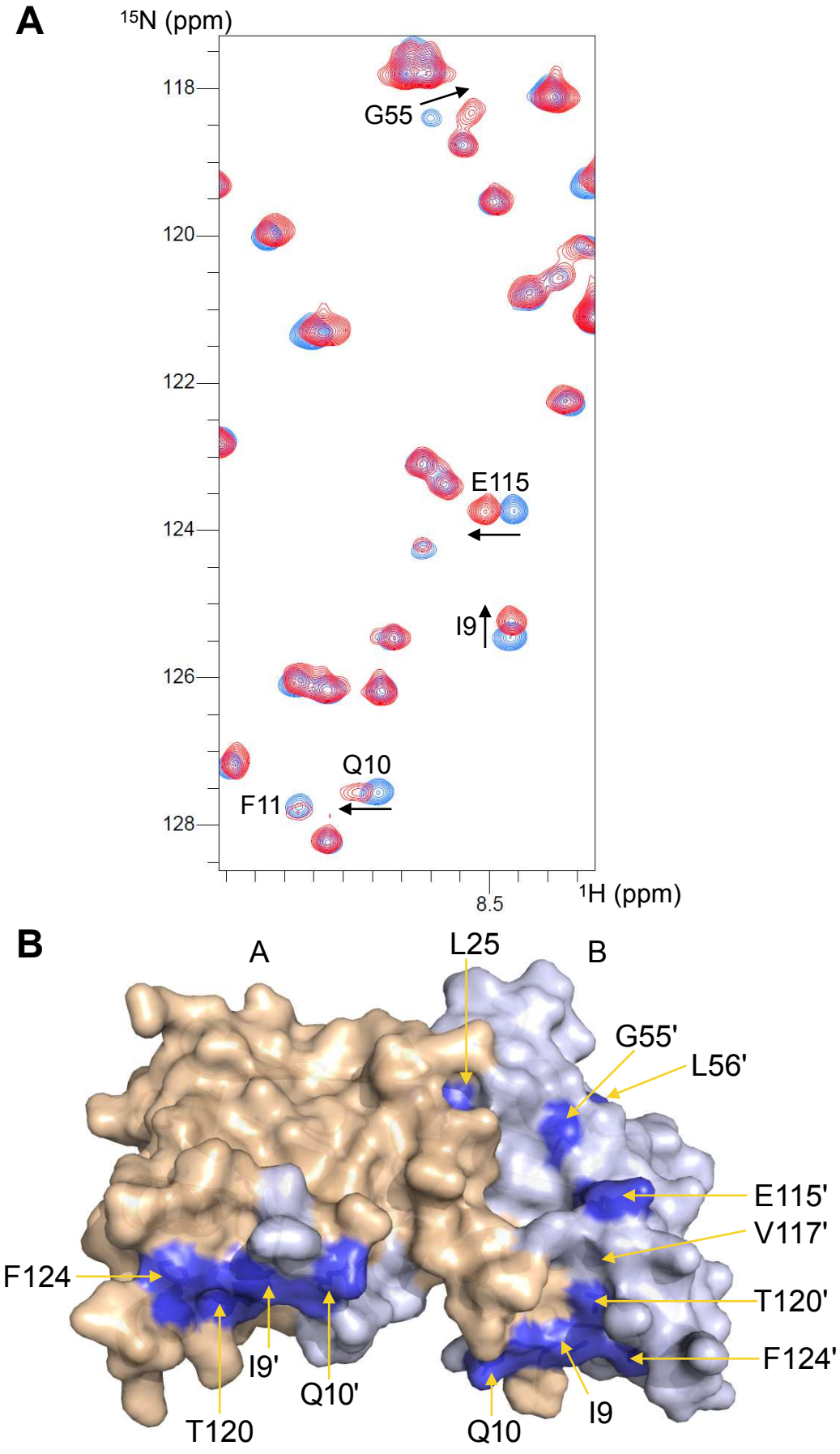
A
15N (ppm)
118
120
122
124
126
128
G55
E115
I9
Q10
F11
8.5
1H (ppm)
B
A
L25
B
G55'
L56'
E115'
V117'
T120'
F124'
F124
I9'
Q10'
T120
Q10
I9

Figure 2

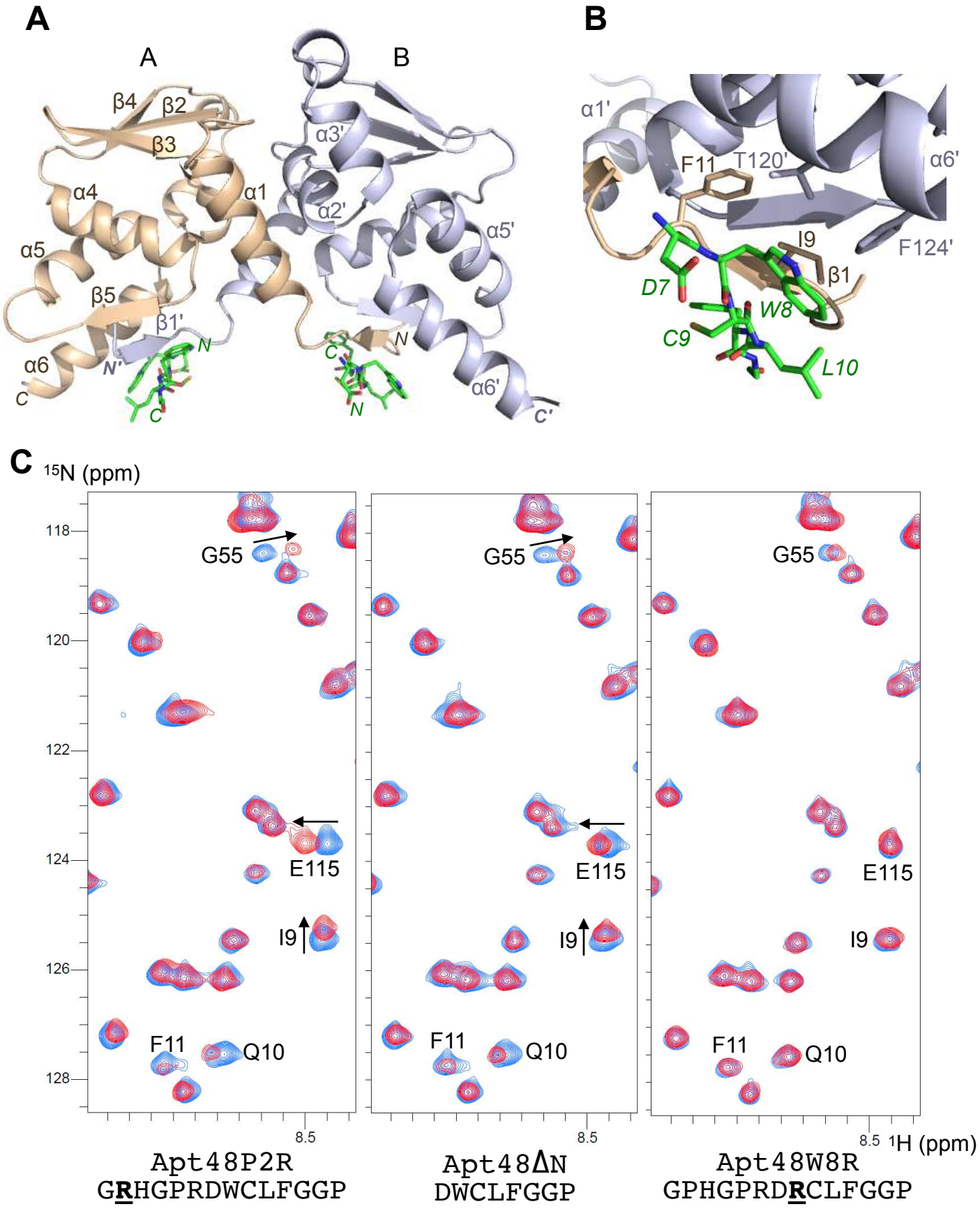
A
A
B
β4
β2
β3
α3'
α4
α1
α2'
α5'
α5
β5
β1'
α6
N'
N
C
C
C
N
α6'
C'
B
α1'
F11
T120'
α6'
I9
F124'
β1
D7
W8
C9
L10
C
15N (ppm)
118
120
122
124
126
128
G55
E115
I9
F11
Q10
8.5
1H (ppm)
Apt48P2R
GRHGPRDWCLFGGP
Apt48ΔN
DWCLFGGP
Apt48W8R
GPHGPRDRCLFGGP

Figure 3

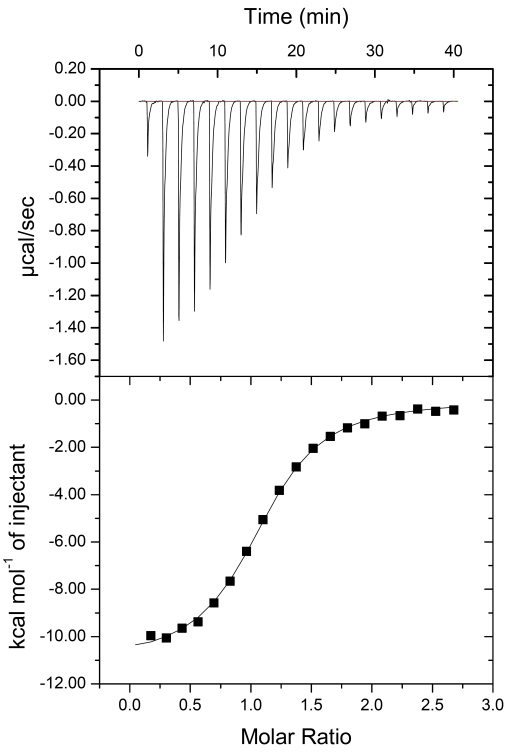

BCL6^{BTB-TM}

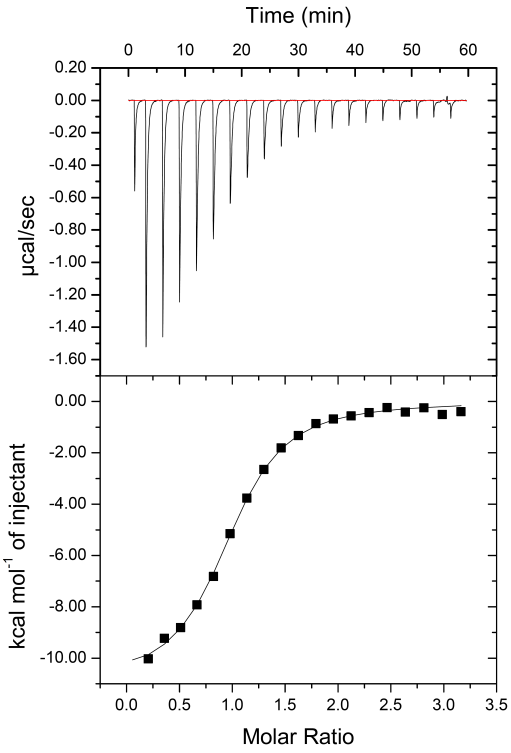

BCL6^{BTB-DM}

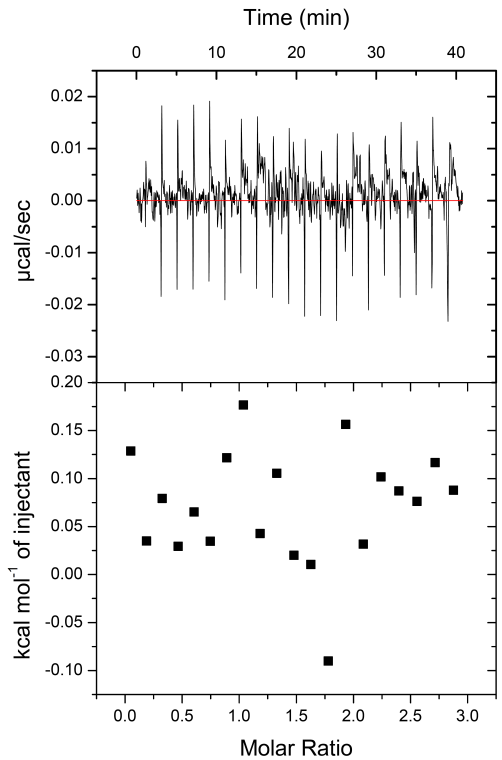

BCL6$^{BTB-DM-I9E}$

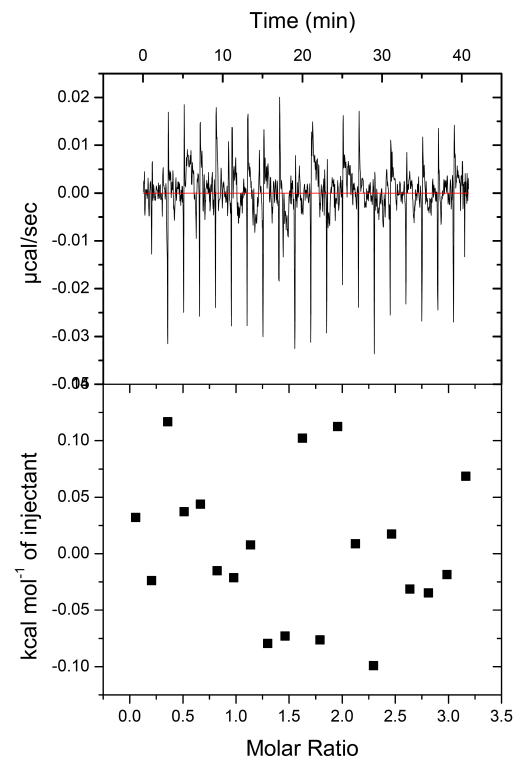

BCL6$^{BTB-DM-F11E}$

Figure 4

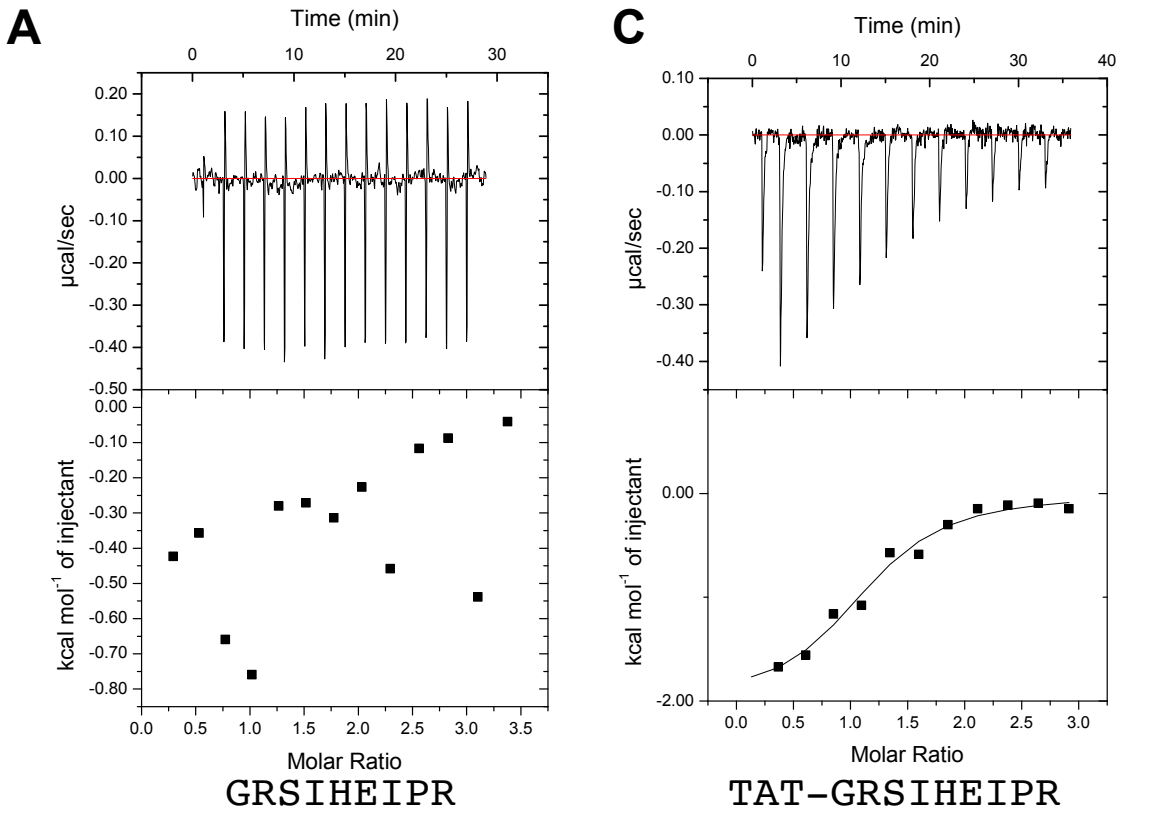
A
Time (min)
µcal/sec
kcal mol-1 of injectant
Molar Ratio
GRSIHEIPR
C
Time (min)
µcal/sec
kcal mol-1 of injectant
Molar Ratio
TAT-GRSIHEIPR

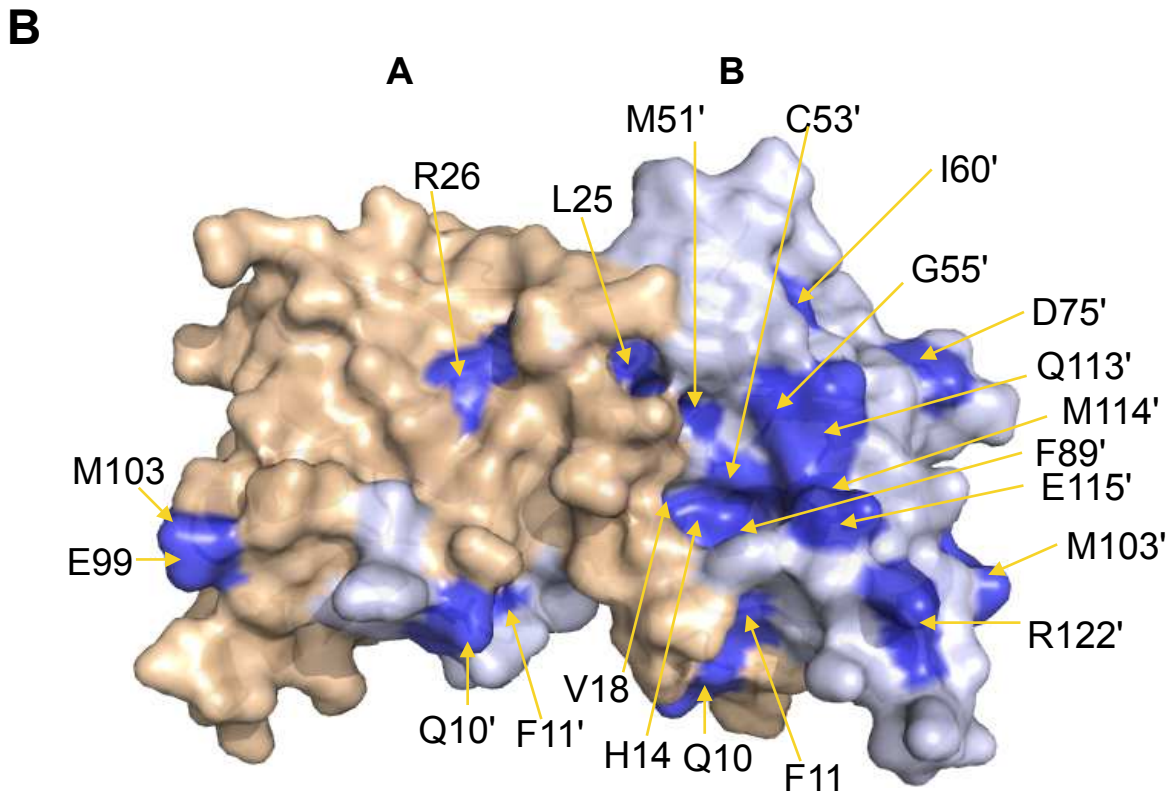
B
A
B
M51'
C53'
I60'
R26
L25
G55'
D75'
Q113'
M114'
F89'
E115'
M103
E99
M103'
R122'
V18
Q10'
F11'
H14
Q10
F11

Figure 5

A

DWCLFGGP Apt48ΔN

GRSIHEIPR truncated SMRT^{BBD}

PGGFLCWDGRSIHEIPR	HBP
LVATVKEAGRSIHEIPR	SMRT
GITTIKEMGRSIHEIPR	NCoR
RSEIISTAPSSWVVPGP	BCOR
LWYTDIRMSWRVP	F1324
YGRKKRRQRRRGGRSIHEIPR	TAT-GRSIHEIPR

B

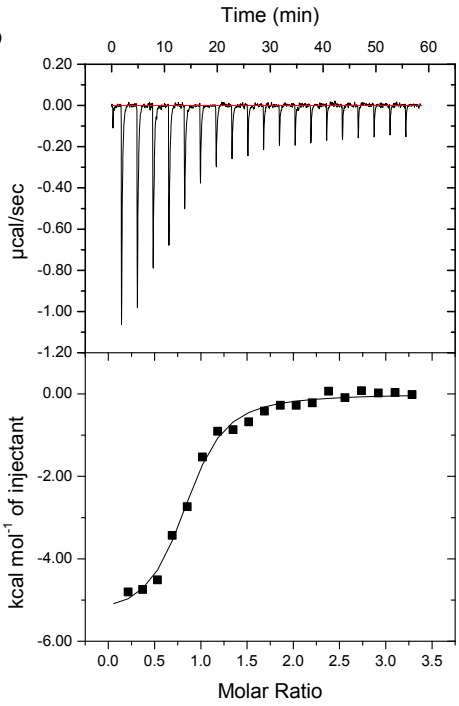

C

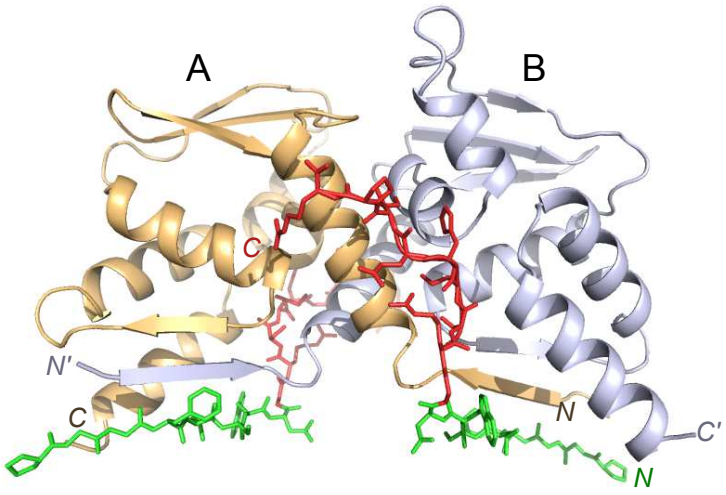

D

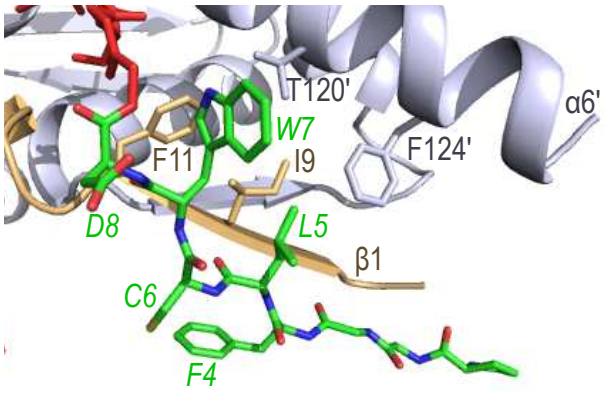

E

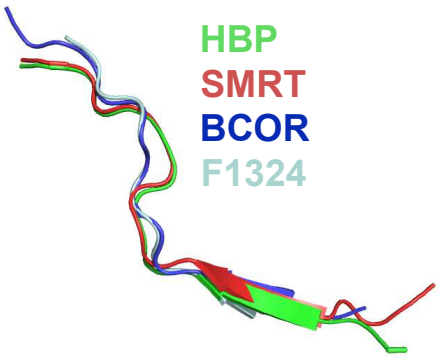

F

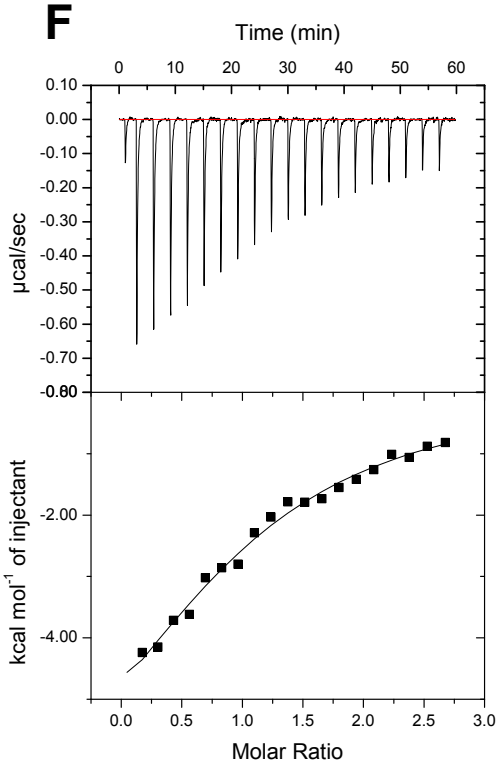

PGGFL<u>RRR</u>GRSIHEIPR

G

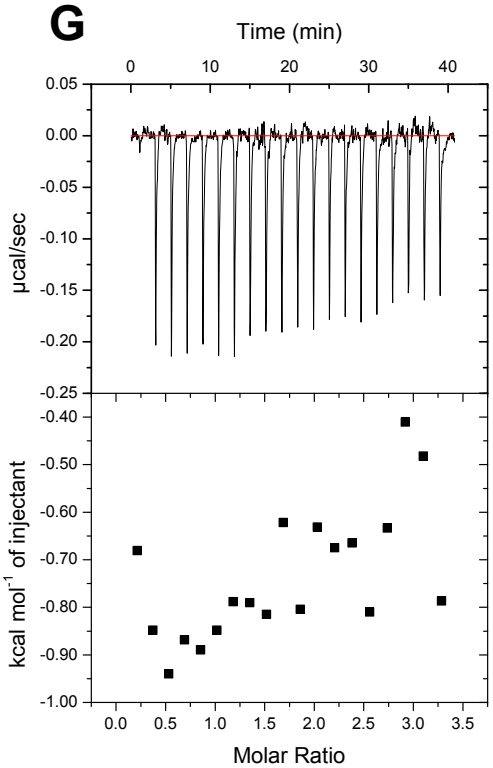

PGGFLCWDGR<u>AA</u>HEIPR

Figure 6

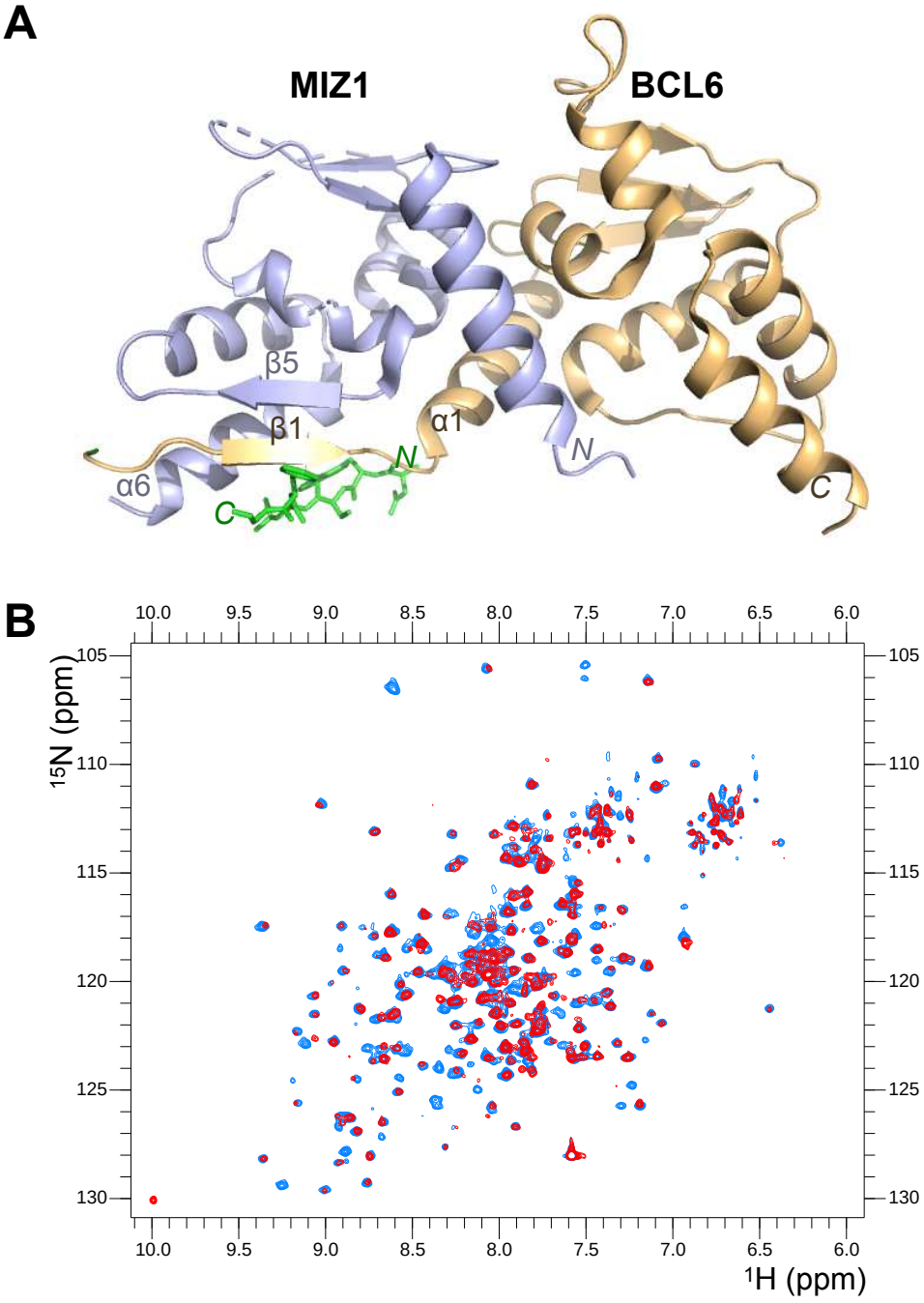
A
MIZ1
BCL6
β5
β1
α1
α6
N
C
N
C
B
10.0
9.5
9.0
8.5
8.0
7.5
7.0
6.5
6.0
105
110
115
120
125
130
15N (ppm)
1H (ppm)

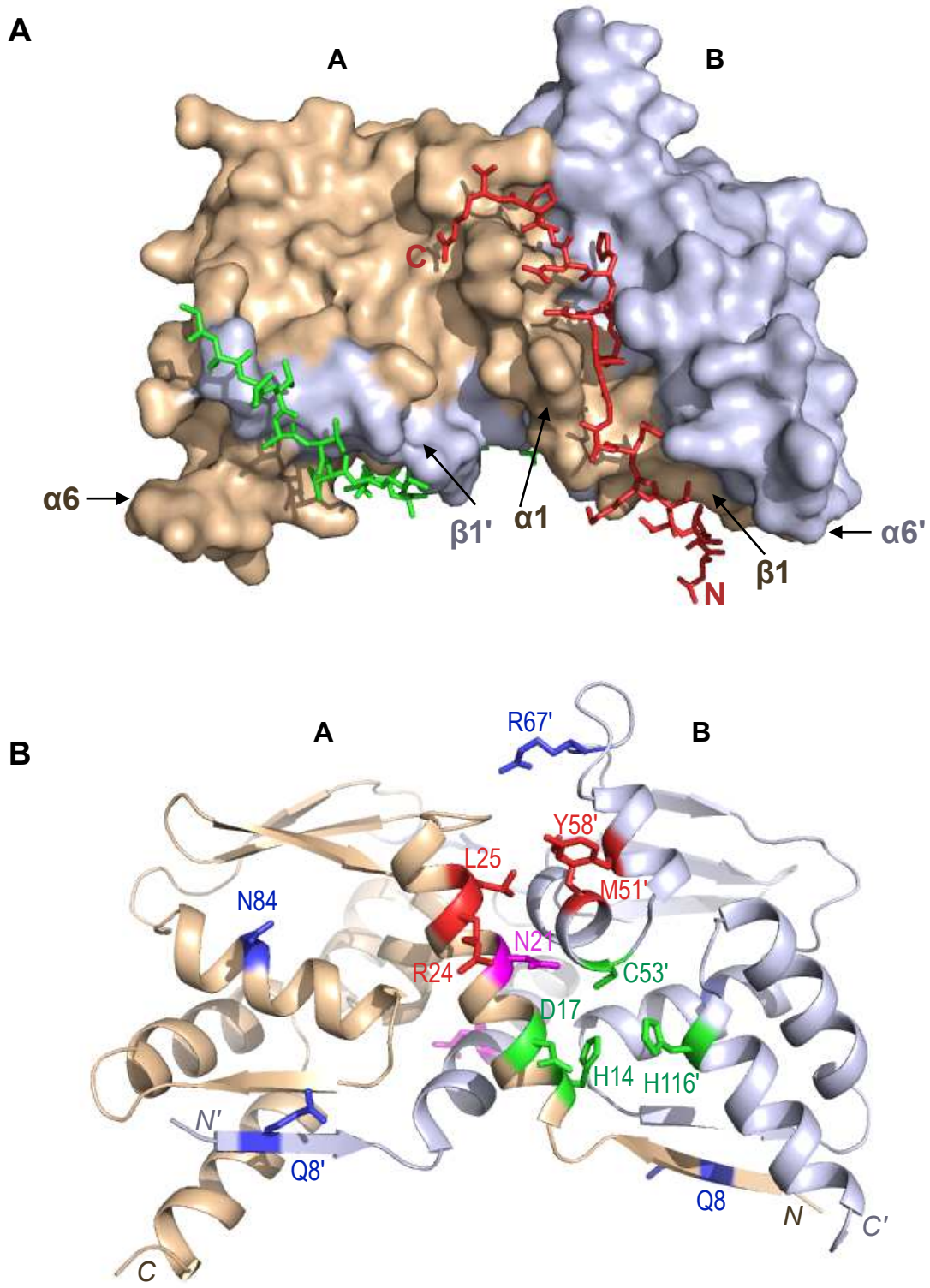

Figure S1. Organisation of the BCL6 BTB domain (related to Figure 1)

A. Surface representation of the previously reported interaction of two SMRT^{BBD} peptide molecules with the BCL6 BTB domain dimer (PDB entry 1r2b; Ahmad et al., 2003). Each peptide molecule interacts with a groove formed at the dimer interface on each lateral surface (the "lateral groove"), and also with the β1−strand located at the "bottom" of the BTB domain. The BTB domain A and B chains are depicted in brown and light blue respectively, and the SMRT chains are in red and green. Secondary structure elements of the B chain are indicated with a prime.

B. Binding sites of known BCL6 inhibitors. Surface cysteine residues that were mutated in BCL6 BTB domain crystal structures are indicated in blue (C8Q, C67R and C84N). Mutation of the lateral groove residue, N21 (magenta), to lysine abolishes interaction with SMRT^{BBD} (Ahmad et. al., 2003). The sites that have been targeted by known inhibitors are indicated on one face of the molecule: residues of the aromatic site (R24, L25, M51' and Y58') are in red, and residues of the HDCH site (H14, D17, C53' and H116') are in green. Residues R67, N84' and N21' are hidden from view on the opposite face of the BTB dimer. This figure was generated using PDB entry 1r2b (Ahmad et al., 2003).

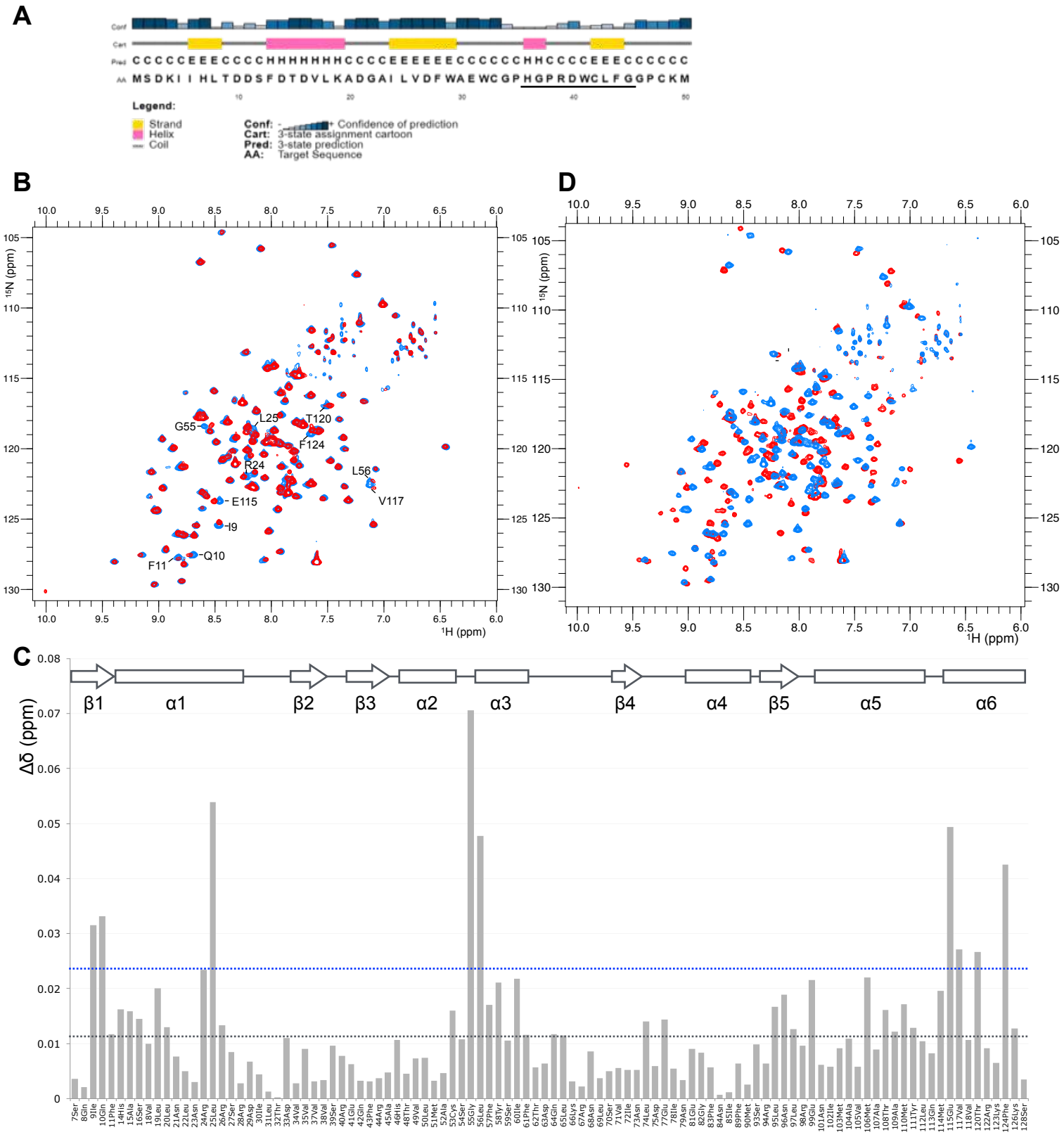

Figure S2. Apt48 binds a lower hydrophobic face of the BCL6 BTB domain (related to Figure 1)

A. Secondary structure prediction of Apt48 (underlined) in the context of the thioredoxin fold, with E=beta strand, H=Helix and C=random coil. Confidence values are given. The prediction was made with the PSIPRED4.0 server (Jones, 1999; Buchan and Jones, 2019).

B. ^{1}H-^{15}N TROSY HSQC spectra of $BCL6^{BTB\text{-}TM}$ in the absence (blue) and presence (red) of an 8−fold molar excess of Apt48 peptide.

C. The chart indicates the resonance shift changes of individual residues of the spectrum depicted in (B); the black broken line indicates 1σ of the mean chemical shift change, and the blue broken line indicates 2σ. The following fifteen BCL6 residues were unassigned in the original spectrum of Lin et. al. (BRMB entry 27079; Lin et al., 2018): 6, 12, 13, 17, 36, 76, 80 86, 87, 88, 91, 92, 100, 116, 129; additionally, the following five residues were not transferred from BRMB entry 27079 to our spectrum: 47, 119, 121, 125, 127.

D. ^{1}H-^{15}N TROSY HSQC spectra of $BCL6^{BTB\text{-}TM}$ in the absence (blue) and presence (red) of a 2-fold molar excess of $SMRT^{BBD}$ peptide.

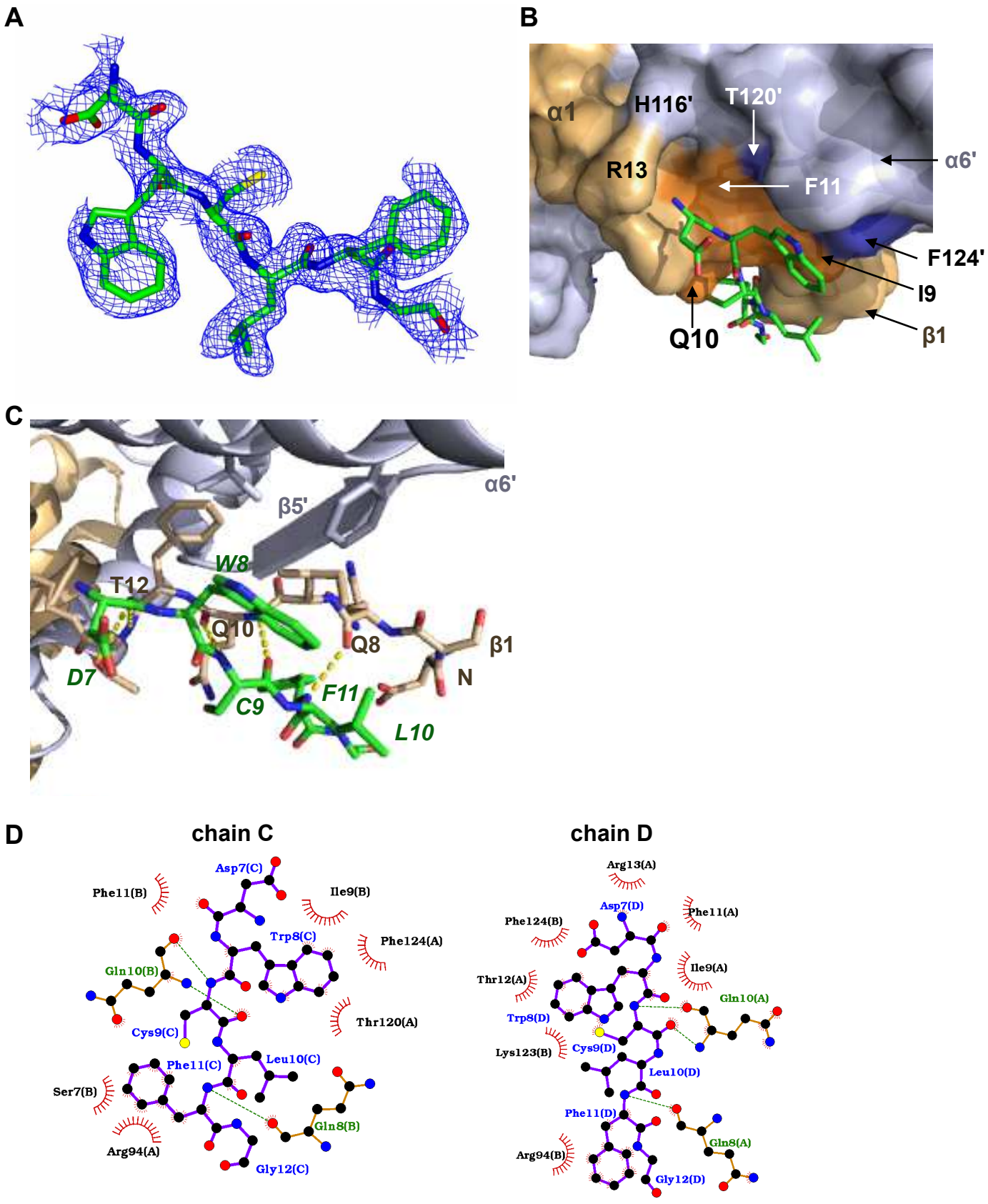

Figure S3. Structure of the BCL6^{BTB-TM}/Apt48 complex (related to Figure 2)

A. Simulated annealing composite omit map of the Apt48 peptide, contoured to 1σ.

B. Surface representation of the binding of Apt48 at the lower portion of the BTB domain. The A and B chains of the BTB domain are in brown and light blue respectively; residues of each chain that show resonance shift changes are indicated in orange and dark blue respectively. The side chains of R13 and H116' are oriented such that the lateral groove is partially "blocked", as observed in some crystal structures of the BTB domain in the absence of co-repressor peptides (e.g. PDB entry 1r29, Ahmad et al., 2003).

C. Interactions between the Apt48 peptide and the BCL6 BTB domain β1−strand. Residues of Apt48 are italicised in green.

D. Schematic drawing of the contacts between Apt48 (chains C and D of the crystal structure) and the BCL6 BTB domain.

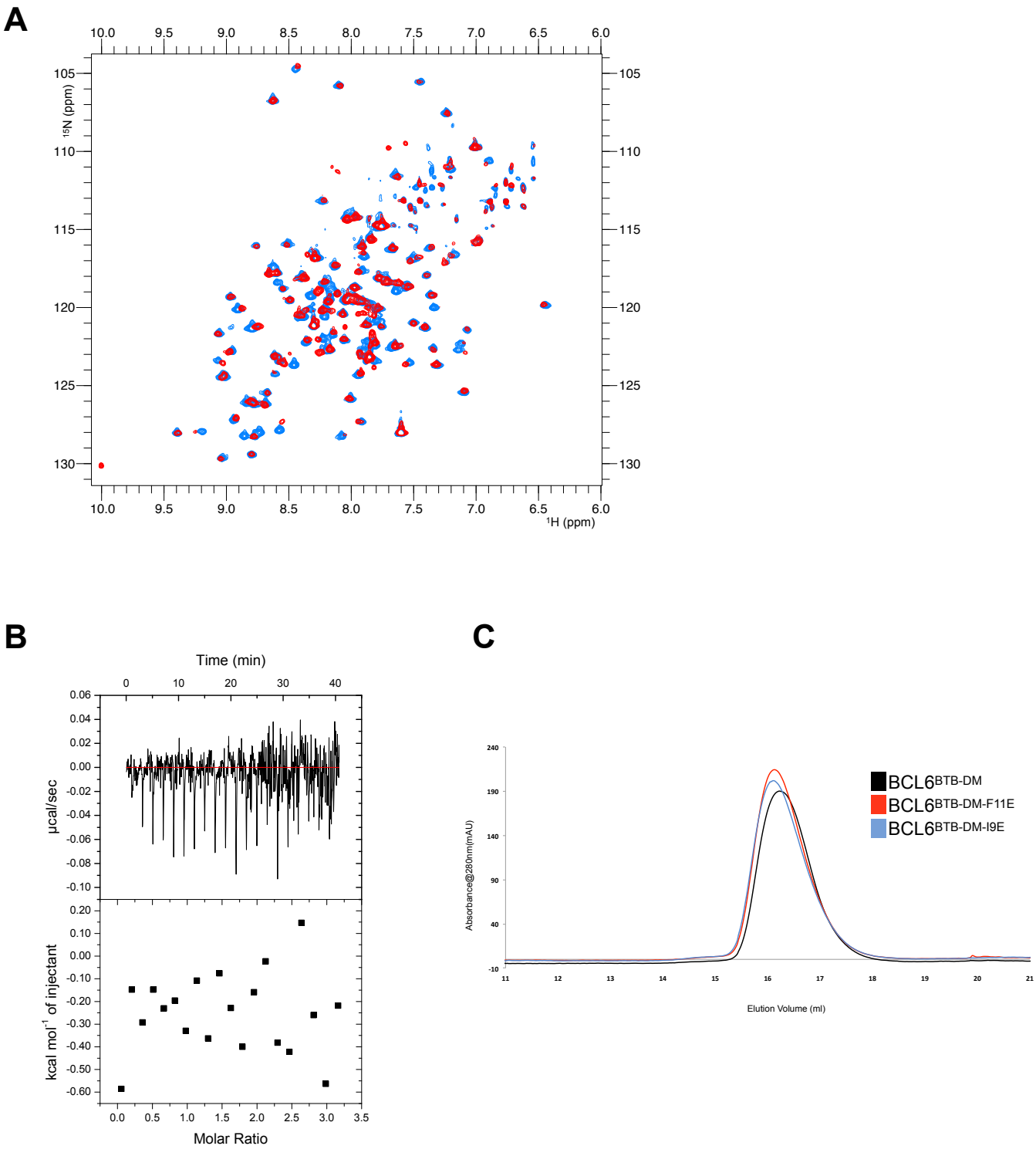

Figure S4. The hydrophobic face of the BCL6 BTB domain is required for interaction with SMRT (related to Figure 3)

A. ^{1}H-^{15}N TROSY HSQC spectra of $BCL6^{BTB\text{-}DM}$ in the absence (blue) and presence (red) of an 8-fold molar excess of Apt48 peptide.

B. ITC titration of the Apt48 peptide into $BCL6^{BTB\text{-}DM}$.

C. Size-exclusion chromatography of $BCL6^{BTB\text{-}DM}$, $BCL6^{BTB\text{-}DM\text{-}I9E}$ and $BCL6^{BTB\text{-}DM\text{-}F11E}$.

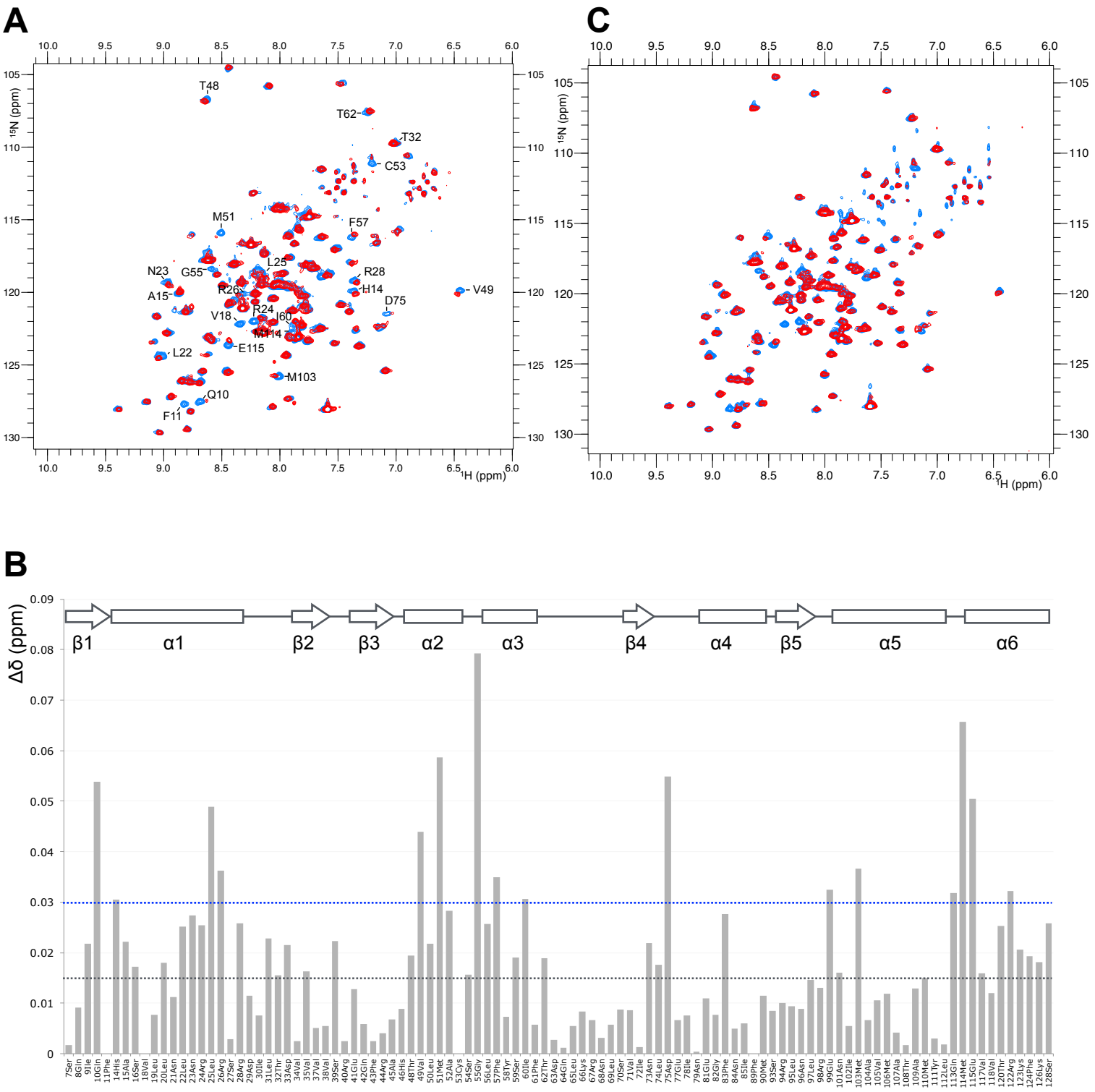

Figure S5. The ^{1}GRSIHEIPR^{9} sequence directs peptide recruitment to the lateral groove (related to Figure 4)

A. ^{1}H-^{15}N TROSY HSQC spectra of BCL6$^{BTB\text{-}TM}$ in the absence (blue) and presence (red) of an 8-fold molar excess of ^{1}GRSIHEIPR^{9} peptide.

B. The chart indicates the resonance shift changes of individual residues of the spectrum depicted in (A); the black broken line indicates 1σ of the mean chemical shift change, and the blue broken line indicates 2σ. Residues F11, V18, C53 and F89 showed broadening.

C. ^{1}H-^{15}N TROSY HSQC spectra of BCL6$^{BTB\text{-}DM}$ in the absence (blue) and presence (red) of an 8-fold molar excess of ^{1}GRSIHEIPR^{9} peptide.

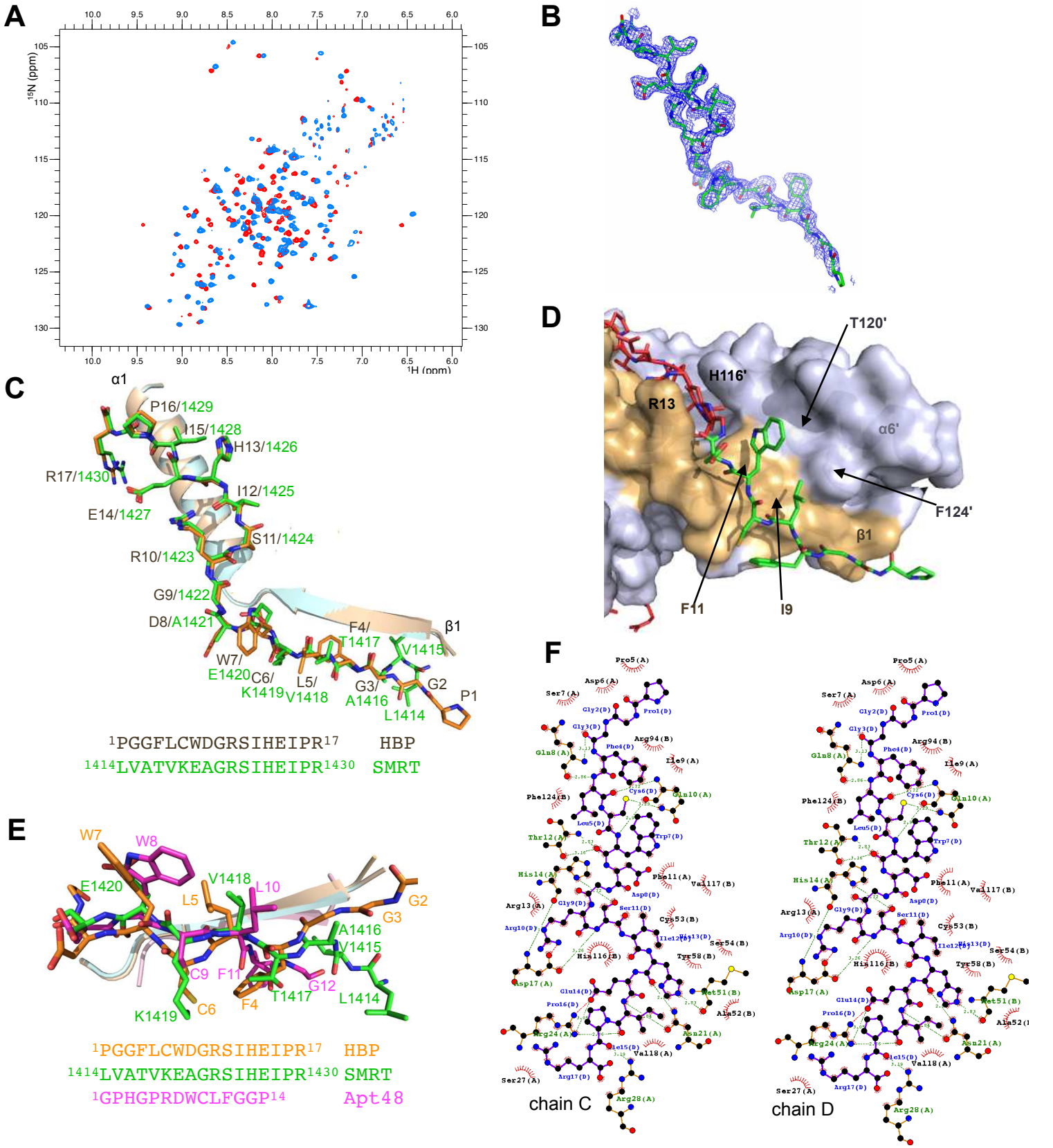

Figure S6. A hybrid BTB-binding peptide (HBP) interacts with the lateral groove (related to Figure 5)

A. ^{1}H-^{15}N TROSY HSQC spectra of BCL6^{BTB-TM} in the absence (blue) and presence (red) of a 2-fold molar excess of HBP peptide .

B. Simulated annealing omit map of the HBP peptide, contoured to 1σ.

C. Structural superposition of the SMRT^{BBD} and HBP peptides. Structures of BCL6^{BTB-TM}/SMRT^{BBD} (PDB entry 1r2b; Ahmad et al. 2003) and BCL6^{BTB-TM}/HBP were superposed by structural alignment of the BTB chains. The α1 and β1 secondary structure elements of the BCL6^{BTB-TM}/SMRT^{BBD} and BCL6^{BTB-TM}/HBP complexes are shown in cyan and brown respectively.

D. Surface representation of the binding of the N-terminal region of the HBP peptide with BTB domain. The A and B chains of the BTB domain are in brown and light blue respectively; the labelled BTB domain residues I9, F11, T120' and F124' form a hydrophobic face that is involved in the interaction with Apt48 (Figure S3B). The side chains of R13 and H116' are oriented away from the lateral groove (contrast Figure S3B).

E. Superposition of the BCL6^{BTB-TM}/SMRT^{BBD} (PDB entry 1r2b; Ahmad et al., 2003), BCL6^{BTB-TM}/Apt48 and BCL6^{BTB-TM}/HPB structures. Superposition was by structural alignment of the β1−strands; the β1−strands and the BTB-interacting peptides are shown.

F. Schematic drawing of the contacts between the HBP (chains C and D of the crystal structure) and the BCL6BTB domain.